NASA Contractor Report 166047

NASA-CR-166047
19830007048

THE USE OF LATERALLY VECTORED THRUST TO COUNTER THRUST ASYMMETRY IN A TACTICAL JET AIRCRAFT

James R. Simons

THE GEORGE WASHINGTON UNIVERSITY
Joint Institute for Advancement of Flight Sciences
Hampton, Virginia 23665

NASA Cooperative Agreement NCC1-29
January 1983

National Aeronautics and Space Administration

Langley Research Center
Hampton, Virginia 23665

TABLE OF CONTENTS

This Page Intentionally Left Blank

LIST OF TABLES

This Page Intentionally Left Blank

LIST OF FIGURES

LIST OF SYMBOLS

Symbols are defined in terms of SI Units with equivalent U.S. Customary Units given parenthetically where appropriate.

b	span, m
C_D	drag coefficient
$C_{D_{C_L}}$	parameter in the $C_D(C_L)$ function, Equation (B-2)
C_L	lift coefficient
C_ℓ, C_m, C_n	generalized aerodynamic moment coefficient about X, Y, Z vehicle reference axes, respectively, $\frac{\text{Moment}}{\bar{q}S\ell}$; body axes moment coefficients
C_X, C_Y, C_Z	generalized aerodynamic force coefficients along X, Y, Z vehicle reference axes, respectively, $\frac{\text{Force}}{\bar{q}S}$; body axes force coefficients
$\bar{c}$	reference chord, m
D	aerodynamic drag, N
F_X, F_Y, F_Z	forces along X, Y, Z vehicle reference axes, respectively, N
$F_{X_p}, F_{Y_p}, F_{Z_p}$	components of thrust (propulsion) along X, Y, Z vehicle reference axes, respectively, N
$\underline{F}$	force vector, where $\underline{F} = F_X\underline{i} + F_Y\underline{j} + F_Z\underline{k}$
g	acceleration due to gravity, m/sec^2
h	altitude, m ($h = -z$)
I_X, I_Y, I_Z	moments of inertia about X, Y, Z vehicle reference axes, respectively, $kg\text{-}m^2$
I_{XZ}	product of inertia, $I_{XZ} = \int xz\, dm$, $kg\text{-}m^2$

$\underline{i},\underline{j},\underline{k}$	unit vectors of orthogonal coordinate system
L	aerodynamic lift, N
ℓ	{length used in nondimensionalizing moments, m characteristic length, m
M_X, M_Y, M_Z	aerodynamic moments about X, Y, Z vehicle reference axes, respectively, N-m
m	instantaneous mass of vehicle, kg
p,q,r	components of angular velocity about X, Y, Z vehicle reference axes, respectively, rad/sec
$\bar{q}$	free-stream dynamic pressure, N/m^2
S	vehicle reference area, m^2
T	total vehicle thrust, N
t	time, sec
u,v,w	components of vehicle absolute (inertial) velocity along X, Y, Z vehicle reference axes, respectively, m/sec
V	resultant velocity, m/sec
W	vehicle weight, N
X,Y,Z	vehicle reference axes
X_e, Y_e, Z_e	right-handed earth fixed axes with origin on earth's surface
x,y,z	distances measured along X_e, Y_e, Z_e earth fixed axes, respectively, m
α	angle of attack, rad
β	angle of sideslip, rad
Γ	transformation matrix for orthogonal axes systems
$\delta_a, \delta_e, \delta_r, \delta_v$	control deflections (aileron, elevator, rudder, vectored thrust, respectively), rad
θ	pitch angle, rad

ρ	atmospheric density, kg/m^3
ϕ	roll angle, rad
ψ	yaw angle, rad
ω	resultant angular velocity, rad/sec

Subscripts:

a	aerodynamic
B	body axes
e	earth axes
g	gravitational
i	inertial
L	lift
mc	minimum for control
o	values of C_L and C_D for $\alpha = 0$
p	propulsive
S	stall
s	stability axes
w	wind axes

Notation:

$\dot{}$	over the symbol indicates the first derivative with respect to time
Δ	perturbation quantity

Abbreviations:

A	Analog
AFCS	Automatic Flight Control System

cg	center of gravity
CPU	Central Processor Unit
ICs	Initial Conditions
I/O	Input/Output
KTAS	Knots True Air Speed, nautical miles per hour
MAC	Mean Aerodynamic Chord
NASA	National Aeronautics and Space Administration
SAS	Stability Augmentation System
TVC	Thrust Vector Control
V/STOL	Vertical/Short Take Off and Landing

Aerodynamic derivatives (referenced to a system of wind and body axes with the origin at the aircraft center of gravity):

$$C_{D_{\delta_r}} = \frac{\partial C_D}{\partial \delta_r} \qquad C_{L_\alpha} = \frac{\partial C_L}{\partial \alpha} \qquad C_{L_{\delta_e}} = \frac{\partial C_L}{\partial \delta_e}$$

$$C_{\ell_p} = \frac{\partial C_\ell}{\partial \frac{pb}{2V}} \qquad C_{\ell_r} = \frac{\partial C_\ell}{\partial \frac{rb}{2V}} \qquad C_{\ell_\beta} = \frac{\partial C_\ell}{\partial \beta}$$

$$C_{\ell_{\delta_a}} = \frac{\partial C_\ell}{\partial \delta_a} \qquad C_{\ell_{\delta_r}} = \frac{\partial C_\ell}{\partial \delta_r} \qquad C_{m_q} = \frac{\partial C_m}{\partial \frac{q\bar{c}}{2V}}$$

$$C_{m_\alpha} = \frac{\partial C_m}{\partial \alpha} \qquad C_{m_{\delta_e}} = \frac{\partial C_m}{\partial \delta_e} \qquad C_{n_p} = \frac{\partial C_n}{\partial \frac{pb}{2V}}$$

$$C_{n_r} = \frac{\partial C_n}{\partial \frac{rb}{2V}}$$

$$C_{n_\beta} = \frac{\partial C_n}{\partial \beta}$$

$$C_{n_{\delta_a}} = \frac{\partial C_n}{\partial \delta_a}$$

$$C_{n_{\delta_r}} = \frac{\partial C_n}{\partial \delta_r}$$

$$C_{Y_\beta} = \frac{\partial C_Y}{\partial \beta}$$

$$C_{Y_{\delta_a}} = \frac{\partial C_Y}{\partial \delta_a}$$

$$C_{Y_{\delta_r}} = \frac{\partial C_Y}{\partial \delta_r}$$

CHAPTER I

INTRODUCTION

Multi-engine aircraft, with engines laterally separated from the aircraft longitudinal axis, experience a yawing moment whenever the engines are not producing equal amounts of thrust. This is normally a liability, the severity of which depends on the: (1) Amount of thrust asymmetry involved; (2) Distance the engines are located from the aircraft centerline; (3) Direction of engine rotation for propellor driven aircraft; (4) Phase(s) of flight involved; (5) Aircraft configuration, including asymmetrical fuel, weapons, or cargo loads as well as the position of flaps, slats, landing gear, etc.; (6) Other aircraft characteristics, including wing loading, total thrust available, center of gravity location, control effectiveness, accompanying loss of systems such as generators, hydraulic pumps, fuel pumps, or other systems which degrade the capability to properly assess and deal with the situation; (7) Environment (terrain obstruction, density altitude, field length, and weather); and, finally, (8) Actions of the pilot.

While the number of variables involved is large, the options available for corrective action are much more limited, and depend primarily on the phase of flight. Phases of flight can be classified as (Ref. 1): (1) Nonterminal flight phases, and (2) Terminal flight phases. Nonterminal flight phases generally involve operations at relatively high airspeed, altitude, and Lift/Drag (L/D) ratios, and low angle of attack,

α, and angle of sideslip, β. For the case of a significant thrust asymmetry (due typically to failure of one or more engines on one side of the aircraft), nonterminal flight phases such as cruise and loiter require corrective actions that are much less urgent than for thrust asymmetry during terminal flight phases. The pilot can even temporarily reduce thrust on the remaining engine(s) to eliminate the thrust asymmetry without immediate fear of striking the earth or exceeding critical values of α or β. There is time to attempt restarts or take other helpful actions without the immediate prospect of losing control.

Terminal flight phases include takeoff, catapult takeoff, approach, wave-off/go-around, and landing. An engine loss can be critical during these phases, where the airspeed, L/D ratio, and altitude are relatively low, and α is relatively high. The corrective actions are urgent, and consist of (in sequence):

(1) Selecting full power on all throttles.

(2) Identifying the dead engine(s) and applying appropriate flight controls:

(A) Rudder as necessary to maintain directional control.

(B) Pitch control as necessary to maintain airspeed above the minimum for directional control (V_{mc}) which is defined as the speed below which the engine out yawing moment can no longer be controlled (some sideslip will exist) using the maximum available rudder deflection. The pitch control must also keep α below stall, and the lift coefficient (C_L)

high enough to prevent the aircraft from losing excessive altitude and striking the earth's surface. Note that the last requirement usually provides a serious conflict with the first two.

(C) Aileron as necessary to counter rolling induced by the yawing moment, and to establish bank angles necessary to maintain directional control.

(3) Making configuration adjustments to reduce the asymmetry, reduce drag, reduce gross weight, reduce stores asymmetry, and so on. This might include feathering a dead propellor, jettisoning external fuel tanks, changing flap settings, retracting the landing gear, closing cowl flaps or speed brakes, or a number of other possibilities depending on the aircraft.

One of the primary reasons why thrust asymmetry can cause a critical situation during terminal flight phases is because the dynamic pressure, which varies as the square of the airspeed, is relatively low. This results in reduced aerodynamic control effectiveness to counter any yawing moment produced by thrust asymmetry, since the yawing moment is relatively independent of dynamic pressure and does not decrease as airspeed is decreased.

The use of vectored thrust to augment or replace aerodynamic controls is not a new concept. The German V-2 rocket of World War II used vanes located in the rocket exhaust to augment the aerodynamic control surfaces (Ref. 2). More recently, the British Hawker-Siddeley "Harrier" V/STOL jet uses thrust vectoring, and was placed in production in 1967.

Since then, a tremendous amount of material has been published concerning the use of vectored thrust in aircraft and missiles. Although most of the work in aircraft thrust vectoring has dealt with vectoring in the pitch plane for maneuver enhancement or improved V/STOL capability, the use of lateral vectoring has not been ignored (Refs. 3-5).

The purpose of this report is to investigate the use of laterally vectored thrust to counter the adverse effects of thrust asymmetry in a twin engine tactical jet, for the case of single engine failure during terminal flight phases.

For this report, the linearized, small perturbation equations of motion were used to predict the steady-state control deflections required for a single engine failure. Then, as explained in Appendices B and C, a full nonlinear six degree-of-freedom simulation was built on a hybrid computer to study transient responses. A hybrid computer was used for three main reasons: (1) The analog portion of the hybrid computer permits simulation of the real physical system as it actually performs (as a continuous system rather than discrete), and allows quick revisions to the system plant without extensive software modifications. The digital portion allows use of a modern digital control system to control the plant. The hybrid computer combines these capabilities and offers built-in analog-to-digital and digital-to-analog signal processing without having to interface analog and digital systems that were not specifically designed to interact. (2) It could easily incorporate a cockpit, with analog displays and controls, at some future time, and

(3) It offered nearly unlimited availability and did not require use of a NASA Langley computer account.

Finally, the simulator transient and steady-state responses were examined for different flight conditions and thrust vectoring parameters, and the results compared to the analytical predictions.

Unlike most American built, propellor driven twin engine aircraft, in which the left engine is the "critical engine," or worst case situation for a single engine failure, jet powered tactical fighters do not have this limitation, and throughout this study only the case of a right engine out will be studied. All results will be assumed to apply equally to a left engine failure.

CHAPTER II

EQUATIONS OF MOTION

The equations of motion for the aircraft can be derived from Newton's Second Law of motion. This is done in most aeronautical engineering textbooks; a thorough treatment is given in Reference 6. The usual assumptions used are: (1) the aircraft is a rigid body; (2) the mass of the aircraft remains constant for each particular flight condition examined, although the mass is different from one flight condition to another; (3) gyroscopic moments are not considered for any engines or rotating machinery on board the aircraft; and (4) the atmosphere is assumed fixed with respect to the earth.

Under these assumptions the equations of motion can be written in the body axes as:

$$\Sigma \Delta F_X = m(\dot{u} + qw - rv) \tag{2-1}$$

$$\Sigma \Delta F_Y = m(\dot{v} + ru - pw) \tag{2-2}$$

$$\Sigma \Delta F_Z = m(\dot{w} + pv - qu) \tag{2-3}$$

$$\Sigma \Delta M_X = \dot{p}I_X - \dot{r}I_{XZ} + qr\left(I_Z - I_Y\right) - pqI_{XZ} \tag{2-4}$$

$$\Sigma \Delta M_Y = \dot{q}I_Y + pr\left(I_X - I_Z\right) + \left(p^2 - r^2\right)I_{XZ} \tag{2-5}$$

$$\Sigma \Delta M_Z = \dot{r}I_Z - \dot{p}I_{XZ} + pq\left(I_Y - I_X\right) + qrI_{XZ} \tag{2-6}$$

The three kinematic equations involved are:

$$\dot{\psi} = (q \sin \phi + r \cos \phi)/\cos \theta \tag{2-7}$$

$$\dot{\theta} = q \cos \phi - r \sin \phi \tag{2-8}$$

$$\dot{\phi} = p + q \sin \phi \tan \theta + r \cos \phi \tan \theta \tag{2-9}$$

Euler angles ψ, θ, and ϕ are defined in Figure 1; angles α and β in Figure 2.

The sense of positive control deflections is also given by Figure 2. Note that the convention differs from NASA standard with regard to aileron deflection.

The equations of motion were incorporated in the simulation through two steps. First, angular rate equations were rewritten from Equations (2-4), (2-5), and (2-6) as:

$$\dot{p} = \left(\frac{I_Y - I_Z}{I_X}\right) qr + \frac{I_{XZ}}{I_X} (\dot{r} + pq) + \frac{M_X}{I_X} \tag{2-10}$$

$$\dot{q} = \left(\frac{I_Z - I_X}{I_Y}\right) rp + \frac{I_{XZ}}{I_Y} \left(r^2 - p^2\right) + \frac{M_Y}{I_Y} \tag{2-11}$$

$$\dot{r} = \left(\frac{I_X - I_Y}{I_Z}\right) pq + \frac{I_{XZ}}{I_Z} (\dot{p} - qr) + \frac{M_Z}{I_Z} \tag{2-12}$$

where body axis moments M_X, M_Y, and M_Z are obtained from the equations:

$$M_X = \bar{q} S b C_\ell + M_{X_p} \tag{2-13}$$

$$M_Y = \bar{q}S\bar{c}C_m + M_{Y_p} \tag{2-14}$$

$$M_Z = \bar{q}SbC_n + M_{Z_p} \tag{2-15}$$

where M_{X_p}, M_{Y_p}, and M_{Z_p} are the propulsive moments.

Secondly, the force equations were transformed from body axes to wind axes, for two reasons: (1) C_L and C_D were available, not C_Z or C_X; and (2) It would be difficult to program on the analog computer the inverse trigonometric functions and square roots needed to solve for α and β when using velocity components in the body axes. The force equations in the wind axes are developed in Appendix A and can be written as:

$$\dot{V} = \frac{F_{X_w}}{m} \tag{2-16}$$

$$\dot{\beta} = p \sin \alpha - r \cos \alpha + \frac{F_{Y_w}}{mV} \tag{2-17}$$

$$\dot{\alpha} = -(p \cos \alpha + r \sin \alpha) \tan \beta + q + \frac{F_{Z_w}}{mV \cos \beta} \tag{2-18}$$

where F_{X_w}, F_{Y_w} and F_{Z_w} are defined in Appendix A.

The equations of motion were completed by the expressions for obtaining the velocity components in the body axes:

$$u = V \cos \alpha \cos \beta \tag{2-19}$$

$$v = V \sin \beta \tag{2-20}$$

$$w = V \sin \alpha \cos \beta \tag{2-21}$$

These components were also transformed into earth axes components by use of Euler angle transformations and then numerically integrated with the digital computer to obtain distances traveled over the earth, and altitude changes. All the necessary state variables for the simulation were then available, and were output to the analog strip chart recorders along with the control variables computed digitally by the Automatic Flight Control System (AFCS) subroutine.

The numerical values needed to generate a particular solution are dependent on the flight condition involved. Aircraft physical characteristics and aerodynamic stability and control derivatives obtained from NASA are given in Appendix B. These data were used to define four straight and level, steady state flight conditions for dynamic analysis. The flight conditions are summarized in Table 1. The rational for selecting these flight conditions is given below. Although the following discussions deal with non-steady, untrimmed operation, the velocities, angles of attack, and weight characteristics of each were used to specify the trimmed, straight and level cases given in Table 1.

The conditions can be described as follows:

CONDITION 1 - This is a "middle-of-the-road" first case. From the NASA data, the stability and control derivatives were approximated as linear functions in the α range from 0 to 20 degrees, so $\alpha = 10$ degrees and a reasonably low value of C_L promised to be the most acceptable place to build and check the simulation. In addition, the available moments of inertia were explicitly given only for this weight distribution of fuel load (See Appendix B).

CONDITION 2 - The weight was increased to include full internal fuel, four radar missiles, full gun ammunition, and one externally mounted centerline tank, minus fuel necessary for engine start and run-up, 15 minutes of deck operations or taxi time, and an acceleration to 79 m/s (154 KTAS). This speed is eight knots above the recommended field takeoff speed for a midrange center of gravity (26 percent MAC). It also approximates a catapult takeoff "end airspeed," which is the airspeed attained by the aircraft at the end of the catapult power stroke. Note that the thrust value given in Table 1 is for steady-state flight and is not representative of takeoff thrust. The inertias for this and the following conditions were calculated in accordance with the discussion of Appendix B.

CONDITION 3 - For the same weight and moments of inertia as Condition 2, the initial speed was set at five knots below the computed takeoff speed. This represents the loss of airspeed normally encountered during a single engine failure while taking off at high gross weights, if corrective action is not prompt and correct. It also represents a common operating point for such an aircraft when involved in the primary mission of air-to-air combat, where a single engine failure at relatively high α and low dynamic pressure can cause loss of directional control and subsequent spin entry.

CONDITION 4 - For the same α as Condition 3, but at a reduced weight representative of a landing approach condition, Condition 4 simulates a single engine failure during a wave-off/go-around maneuver.

CHAPTER III

STATIC CONTROL

In order to analytically determine control deflection requirements for a single engine failure without resorting to analog or digital computation, the nonlinear Equations (2-2), (2-4), and (2-6) must be linearized. If this is done, it is possible to quickly obtain solutions which can be used to direct the research effort, or to verify the computer solutions obtained from the nonlinear equations. The linearized, steady-state equations for the lateral motion were used. These equations were obtained from the general equations by incorporating two assumptions: (1) the aircraft motion is restricted to small perturbations from a reference condition of symmetric steady flight with no angular velocities; and (2) since the perturbations are assumed small, the products of perturbations can be neglected.

The form of the linearized equations defining steady sideslip is:

$$\frac{-F_{Y_p} - mg \cos\theta \cdot \phi}{qS} = C_{Y_\beta}\beta + C_{Y_{\delta_r}}\delta_r + C_{Y_{\delta_a}}\delta_a \qquad (3\text{-}1)$$

$$\frac{-M_{X_p}}{\bar{q}Sb} = C_{\ell_\beta}\beta + C_{\ell_{\delta_r}}\delta_r + C_{\ell_{\delta_a}}\delta_a \tag{3-2}$$

$$\frac{-M_{Z_p}}{\bar{q}Sb} = C_{n_\beta}\beta + C_{n_{\delta_r}}\delta_r + C_{n_{\delta_a}}\delta_a \tag{3-3}$$

Since the thrust vector lies in the X-Y plane of the aircraft and was not vectored in the pitch plane, $M_{X_p} = 0$. When the thrust is asymmetric and non-vectored $F_{Y_p} = 0$, because the non-vectored thrust line is assumed parallel to the X axis. For Equations (3-1) through (3-3), all the parameters except ϕ, β, δ_r, and δ_a are known for each trimmed initial flight condition.

The AFCS was designed to use bank angle and rudder and aileron deflection to achieve $\beta = 0$. Equations (3-1), (3-2), and (3-3) can be rewritten to represent this condition, which leaves three linearly independent equations in three unknowns (ϕ, δ_r, δ_a) to be solved simultaneously. These equations can be written in a state-space equation of the form $\underline{y} = A\underline{x}$, where

$$\underline{y} = \begin{bmatrix} \dfrac{-F_{Y_p}}{\bar{q}S} \\ 0 \\ \dfrac{-M_{Z_p}}{\bar{q}Sb} \end{bmatrix}$$

$$A = \begin{bmatrix} \frac{mg\ \cos\theta}{\bar{q}S} & C_{Y_{\delta_r}} & C_{Y_{\delta_a}} \\ 0 & C_{\ell_{\delta_r}} & C_{\ell_{\delta_a}} \\ 0 & C_{n_{\delta_r}} & C_{n_{\delta_a}} \end{bmatrix}$$

$$\underline{x} = \begin{bmatrix} \phi \\ \delta_r \\ \delta_a \end{bmatrix}$$

Then $\underline{x} = A^{-1}\underline{y}$.

Calculations with an engine out for both the non-vectored case and the case when the remaining thrust is vectored 5.7 degrees (through the aircraft center of gravity) resulted in control deflections as shown in Table 2.

The calculations indicate that vectoring the thrust will eliminate the requirement for rudder and aileron deflections, and also reduce the required bank angle slightly. Although the elimination of aileron deflection is hardly significant, since the greatest deflection required for the non-vectored case is still less than 1 degree, the elimination of 13.5 degrees of rudder deflection is a significant achievement (maximum rudder deflection possible is 30 degrees).

CHAPTER IV

DYNAMIC CONTROL

Once the basic aircraft simulator had been built and the fundamental modes of longitudinal and lateral motion verified, it then became necessary to control the dynamic motion of the aircraft. If subjected to thrust asymmetry without an active controller, the aircraft flight path would quickly diverge from the initial trimmed state, and the aircraft would "crash." In order to control sideslip, bank angle, and all other parameters of interest, it was necessary to provide control, either by having a pilot manually supply control inputs through an analog cockpit connected to the simulator, or by programming an automatic controller to perform the same tasks. For this early stage of the simulator's maturity, the automatic controller was chosen in order to bypass the additional engineering a cockpit would have required, and in order to remove the variability of human response. A block diagram of the automatic controller is given as Figure 3. The automatic controller is labeled "AFCS" (Automatic Flight Control System), and incorporates a Stability Augmentation System (SAS) with inner loops to augment basic aircraft stability and control, and an Autopilot with outer loops for flight path control. As shown, the SAS provides phugoid damping, Dutch roll damping, roll rate damping, and sideslip control, while the Autopilot provides altitude hold, heading control, and wing leveling.

As explained in Appendix C, the Pacer 100 Digital Processor was

used to accomplish the SAS and Autopilot functions, as well as to provide the additional functions of engine dynamics control and Thrust Vector Control (TVC) shown in the "Thrust modes" block of Figure 3.

Since the TVC mode is of primary importance for this report, an introductory discussion is in order.

If thrust is to be vectored, there are two fundamentally different types of control that can be used. The first is a fully active, closed-loop controller that can be used to provide or augment directional stability, as outlined in Reference 4. That report employed a non-specific two-dimensional TVC nozzle, which is a typical approach for a fully active system. The second type is an open-loop controller that is not used unless activated by the pilot or another control system in response to an engine out. An open-loop controller can make use of a simpler vane system that is external to the exhaust jet, and which does not interfere with the exhaust jet during normal twin engine operations. Research is currently being conducted in this area (Ref. 7), and one possible scheme employs two vanes deflected simultaneously and equally when activated (see Figure 4). In this way, no matter which engine failed, thrust from the remaining engine would be vectored through the aircraft cg. Also, in case of inadvertent activation, the net result would only be a small percentage loss of longitudinal thrust component (0.5 percent for a thrust vector angle of 5.7 degrees, not including any efficiency losses). This study used an open-loop controller to drive an external vane system, because of the simplicity and inherent safety.

The Thrust Vector Controller was incorporated in the simulation

as shown in Figure 3. Three decisions were made for each digital $\delta_{T_{command}}$ going from the AFCS to the "Thrust mode" controller. These were open-loop decisions; i.e., independent of AFCS inputs or outputs or of the parameters generated by the aircraft simulation. These decisions were made by the person operating the simulation, through three switches located on the Digital Processor console, and shown schematically in Figure 3. The experimenter could select various combinations of the thrust modes shown. One switch, when activated, set the right engine thrust equal to zero. A second switch either activated TVC logic, or else bypassed it in order to keep the thrust conventionally non-vectored. A third switch controlled selection of the thrust "command double," which will be explained later. If the experimenter activated TVC logic, the computer required three additional pieces of information: (1) The desired reaction delay time, from the moment of single engine failure until the vanes begin to deflect; (2) the actuation interval, or time that it takes the vanes to fully deflect the thrust vector once the vanes begin to move; and (3) the desired thrust vector angle, δ_v, which will vector the thrust through the aircraft cg. This angle can be calculated from the aircraft geometry as shown in Figure 4.

This report does not address the efficiency of the vanes in turning the thrust vector. Based on results reported in Reference 7, it is assumed that a thrust vector angle of 5.7 degrees for this aircraft can be achieved with vane deflection angles less than 10 degrees.

At this point, since a known constant δ_v is assumed, the parameters involved in investigating the engine out case are five-fold:

(1) Which flight condition introduced in Chapter III is being considered;

(2) Whether or not the remaining thrust will be vectored in response to an engine out;

(3) If vectored, the reaction delay time used, as well as

(4) The actuation interval used, and

(5) Whether or not the thrust command double was used.

After obtaining baseline data runs for each of the four flight conditions without thrust vectoring, the TVC was used on all remaining runs. Reaction delay times used were two and four seconds, since only one second is an unrealistically short time for a pilot to identify an engine out condition and activate a control system. Actuation interval times used were one and two seconds, since four or more seconds to move a vane 10 degrees or less is uncharacteristically slow. Each combination mentioned above was run both with and without the thrust command double.

The reason for the thrust command double is as follows: If only the altitude error and phugoid damping requirements are used to generate a thrust command, the thrust response is too slow, and excessive altitude is lost when an engine is cut. Therefore, a mode was added which, when selected, doubled the commanded thrust of the remaining engine as soon as the reaction delay time expired. This commanded thrust was still subject to the engine dynamic limitations, but it quickly increased thrust from the single engine in order to equal the initial value of total thrust from both engines. This type of response is closely akin

to a normal pilot's reaction to an engine out case, when all throttles are immediately advanced to full power, before identifying which engine failed.

For the five parameters mentioned, there are a total of four baseline non-vectored cases to consider, and 32 vectored cases, for a total of 36. These test cases are denoted by an "X" in Table 3, the test matrix.

The results will be presented in Chapter V by first examining the baseline non-vectored cases for each of the four flight conditions, and then investigating the effect of parameter variations. Use of the command double is investigated first, followed by a systematic variation of actuation interval and reaction delay times.

CHAPTER V

RESULTS AND DISCUSSION

Figures 7 through 14 show the time histories for the baseline non-vectored cases of the four chosen flight conditions. The transient peak values and steady-state values are summarized in Table 4(a), and the steady-state values of ϕ, δ_r, and δ_a agree well with the calculated values in Table 2. Conditions 3 and 4 have the largest peak and steady-state values, and, except for altitude perturbations (Δz), the steady-state values of interest for Conditions 3 and 4 are equal, and peak values are very similar. This was also true for the thrust vectored cases. Steady-state values of ϕ, β, δ_r, and δ_a for the thrust vectored cases are shown in Table 4(b), and also agree well with the calculated values in Table 2.

The only figures for vectored thrust that are included in this report are for Condition 3, in order to avoid duplication of Condition 4, and in order to represent the worst overall condition to have to control. Also, Condition 3 figures are restricted to the case for the shortest vectored response time (2 sec reaction delay/1 sec actuation interval) and the case for the longest vectored response time (4 sec reaction delay/2 sec actuation interval). Intermediate cases were redundant.

Since the peak transient values of lateral variables for Condition 4 are slightly greater than for Condition 3, with steady-state values

being equal, the problem of providing lateral mode stability and control is just as great at the reduced weight and speed representing a landing approach (Condition 4) as for the higher gross weights associated with a takeoff (Condition 3). Of course, the descent rates and altitude losses are not as great for the reduced weight condition, but any given propulsive yawing moment can produce higher values of p and r in the condition with the lower weight and moments of inertia.

As explained on page 17 of Chapter IV, it was necessary to use the thrust command double to prevent unacceptable altitude losses in all the flight conditions. Examination of Condition 3 (which has the highest combination of weight and α) emphasizes this necessity: Figure 11 shows an altitude perturbation of 450 m (1476 ft) for the baseline non-vectored case of Condition 3, which does not use the thrust command double. In fact, the maximum available thrust of the remaining single engine at military power [67,500 N (15,175 lb)] is just adequate to cancel the descent rate incurred from the single engine failure, and the simulated aircraft maintains level flight 400 m (1312 ft) below the initial altitude, because there is no excess thrust to regain the altitude lost. When the thrust command double is used with Condition 3, as shown in Figure 17, the altitude perturbation is only 50 m (164 ft). The quicker engine response is important in providing safety margins and pilot acceptance, and should be incorporated in any investigation of the longitudinal or lateral variables. Use of the command double caused greater perturbations in the lateral variables, which can be seen by examining Figures 16, 18, 20, and 22 (the data are summarized in Table 5).

This increase averaged 10 percent for the worst case of the study, but this is acceptable in light of the altitude considerations.

Although use of thrust vector control can eliminate the need for lateral steady-state aerodynamic control deflections, it is important to also consider the effects of TVC on longitudinal performance. As mentioned on page 14 of Chapter IV, 5.7 degrees of vectoring does decrease the longitudinal thrust component by 0.5 percent. Comparison of Figures 11, 15, and 19 (for which the appropriate variables are summarized in Table 6) shows that this decrease is more than offset by benefits derived from thrust vectoring: (a) Eliminating the lateral steady-state aerodynamic control deflections reduces the aircraft drag by approximately 1.4 percent; and (b) The maximum bank angle is reduced from 30 degrees to 14.5 degrees, and comparison of Figures 12 and 16 shows that the area under the curve for bank angle is approximately one-fifth as great as for the non-vectored case. This translates into more effective lift and less altitude lost as a result of bank excursions.

Therefore, the net result of TVC on longitudinal variables for this aircraft is to enhance performance. An equivalent 1.4 percent loss in longitudinal thrust component occurs for a thrust vector angle of 9.6 degrees, implying that vector angles less than that offer potential for improving longitudinal performance.

Finally, the effect of larger reaction delay and actuation interval times is to increase the peak values of the lateral variables while degrading longitudinal performance. This statement can be generalized to include all four flight conditions. Of note here is that the δ_a for

Conditions 3 and 4 reaches the physical limit of 20 degrees deflection for both the non-vectored case, and the vectored case with a 4 second reaction delay. δ_a is saturated for approximately 16 seconds in the non-vectored case and 3.5 seconds in the vectored case. By using a reaction delay of 2 seconds with the TVC, control surface saturation is totally avoided.

CHAPTER VI

CONCLUDING REMARKS

The purpose of this report was to investigate the use of laterally vectored thrust to counter the adverse effects of thrust asymmetry in a twin engine tactical jet, for the case of single engine failure while operating at relatively low airspeeds and L/D ratios typically encountered in landings, takeoffs, and air combat maneuvering. There were several results of the research effort: (1) The linearized, steady-state, lateral equations of motion (used to analytically determine the control deflections required for the engine out case) closely predicted the results provided by flight simulation; (2) The non-linear, six degree-of-freedom simulator that was built on a hybrid computer accurately represents the modeled aircraft for values of α from 0 to 20 degrees (based on comparisons of the simulator's fundamental modes of longitudinal and lateral motion with known values for the data used), and it will provide a flexible tool for further studies of vectoring the thrust laterally, vertically, or in combination. The simulator has the potential to include a piloted cockpit, and to operate at greatly increased values of α; (3) For the flight conditions and aircraft geometry investigated, laterally vectoring the thrust 5.7 degrees, within three seconds of engine failure, required peak rudder deflections less than half that needed when thrust was not vectored, and reduced steady-state deflection from 13.5 degrees to zero. Thrust vectoring similarly

reduced maximum bank angles and heading errors by less than half, while preventing saturation in aileron deflection.

From these results, several conclusions can be drawn for the case of single engine failure in the aircraft studied:

(1) Lateral thrust vectoring can provide significantly decreased peak values of rudder and aileron deflection, heading error, bank angle, and yaw rate. It can eliminate the requirement for significant steady-state rudder deflection.

(2) For relatively small thrust vector angles, the decrease in the longitudinal thrust component caused by the change in the thrust direction can be offset by improved aerodynamic efficiency of the airplane because the aerodynamic controls return to their neutral positions. This assumes that the thrust vectoring device is perfectly efficient in changing the thrust direction.

(3) The reaction delay time (from the moment of single engine failure until the thrust begins to be vectored) is an important parameter which ideally is zero (no delay). If the reaction delay is too long, lateral aerodynamic control saturation may be encountered, even though the vectoring will eventually reduce steady-state deflection requirements to zero if the aircraft does not go out of control.

(4) Single engine failure during the relatively low weight landing approach flight condition can present lateral stability and control problems equal to or worse than those encountered during takeoff at higher weights.

Based on the results and conclusions, laterally vectored thrust

appears to offer a number of additional potential advantages: (a) The ability to augment directional stability through a closed-loop, active controller, thereby decreasing vertical stabilizer size, which offers weight savings and reduced drag; (b) The ability to generate anti-spin moments, thereby lessening the potential for aircraft loss from out-of-control flight; (c) The ability to generate side-force components without bank angles, which could improve an aircraft's capability to handle crosswinds during landing approaches to an airfield, and to make lineup corrections during approaches to an aircraft carrier; and (d) Maintenance of controllability and directional stability at significantly increased α and lower dynamic pressure could play a large role in safely lowering operating speeds during terminal flight phases or air combat maneuvering, either one of which can enhance the effectiveness of a tactical jet aircraft.

APPENDIX A

DEVELOPMENT OF FORCE EQUATIONS

From Newton's Second Law of motion:

$$\Sigma \Delta \underline{F} = m \left.\frac{d\underline{V}}{dt}\right|_e \tag{A-1}$$

In the wind axes:

$$m\underline{g}_w + \underline{F}_{a_w} + \underline{F}_{p_w} = m\left(\frac{d\underline{V}}{dt} + \underline{\omega}_w \times \underline{V}\right) \tag{A-2}$$

where from Reference 6:

$$\underline{\omega}_w = p_w\underline{i} + q_w\underline{j} + \underline{r}_w\underline{k} \tag{A-3}$$

$$\underline{V} = V\underline{i} \tag{A-4}$$

$$p_w = p \cos\alpha \cos\beta + (q - \dot{\alpha})\sin\beta + r \sin\alpha \cos\beta \tag{A-5}$$

$$q_w = -p \cos\alpha \sin\beta + (q - \dot{\alpha})\cos\beta - r \sin\alpha \sin\beta \tag{A-6}$$

$$r_w = -p \sin\alpha + r \cos\alpha + \dot{\beta} \tag{A-7}$$

$$\underline{g}_w = \Gamma_{wB}\Gamma_{Be}\,\underline{g} \tag{A-8}$$

$$\underline{F}_{a_w} = -D\underline{i} + F_{Y_B} \cos\beta\, \underline{j} - L\underline{k} \tag{A-9}$$

$$\underline{F}_{p_w} = \Gamma_{wB}\underline{F}_{p_B} \tag{A-10}$$

$$\Gamma_{Be} = \begin{bmatrix} \cos\psi\cos\theta & \sin\psi\cos\theta & -\sin\theta \\ -\sin\psi\cos\phi + \cos\psi\sin\theta\sin\phi & \cos\psi\cos\phi + \sin\psi\sin\theta\sin\phi & \cos\theta\sin\phi \\ \sin\psi\sin\phi + \cos\psi\sin\theta\cos\phi & -\cos\psi\sin\phi + \sin\psi\sin\theta\cos\phi & \cos\theta\cos\phi \end{bmatrix} \tag{A-11}$$

$$\Gamma_{wB} = \begin{bmatrix} \cos\beta\cos\alpha & \sin\beta & \cos\beta\sin\alpha \\ -\sin\beta\cos\alpha & \cos\beta & -\sin\beta\sin\alpha \\ -\sin\alpha & 0 & \cos\alpha \end{bmatrix} \tag{A-12}$$

After appropriate substitutions:

$$\dot{V} = \frac{F_{X_w}}{m} \tag{A-13}$$

$$\dot{\beta} = p\sin\alpha - r\cos\alpha + \frac{F_{Y_w}}{mV} \tag{A-14}$$

$$\dot{\alpha} = -(p \cos \alpha + r \sin \alpha) \tan \beta + q + \frac{F_{Z_w}}{mV \cos \beta} \tag{A-15}$$

where

$$F_{X_w} = mg \cos \beta(\cos \theta \cos \phi \sin \alpha - \sin \theta \cos \alpha) + mg \sin \beta \cos \theta \sin \phi + \bar{q}S(C_Y \sin \beta - C_D \cos \beta) + \cos \beta\left(F_{X_p} \cos \alpha + F_{Z_p} \sin \alpha\right) \tag{A-16}$$

$$F_{Y_w} = mg \sin \beta(\sin \theta \cos \alpha - \cos \theta \cos \phi \sin \alpha) + mg \cos \beta \cos \theta \sin \phi + \bar{q}S(C_D \sin \beta + C_Y \cos \beta) - \sin \beta\left(F_{X_p} \cos \alpha + F_{Z_p} \sin \alpha\right) \tag{A-17}$$

$$F_{Z_w} = mg(\cos \theta \cos \phi \cos \alpha + \sin \theta \sin \alpha) - \bar{q}SC_L - F_{X_p} \sin \alpha + F_{Z_p} \cos \alpha \tag{A-18}$$

APPENDIX B

CHARACTERISTICS OF AN ADVANCED FIGHTER

Aircraft physical characteristics and aerodynamic stability and control derivatives were obtained from NASA for a representative swept-wing, Mach 2 class twin engine fighter at one operating weight. The physical characteristics are:

$S = 56.48\ m^2$

$\bar{c} = 4.86\ m$

$b = 13.10\ m$

$m = 16{,}280\ kg$

$W = 159{,}652\ N$

$I_X = 34{,}574\ kg\text{-}m^2$

$I_Y = 225{,}900$

$I_Z = 253{,}540$

$I_{XZ} = -13{,}558$

$\ell_X = 7.0\ m$ (longitudinal distance from exhaust nozzle exit plane to aircraft cg)

$\ell_Y = 0.7\ m$ (lateral distance from center of exhaust nozzle to aircraft centerline)

Basic aircraft weight without fuel is approximately 122,500 N (27,539 lb).

Since moments of inertia are proportional to the mass involved, and proportional to the square of the radius arm involved, it was assumed that the relative distribution of any fuel loads different from that originally given would be the same as the original distribution, though the mass would differ. Scaling the moments of inertia

to the relative masses chosen in Chapter II for the four different test conditons results in the moments of inertia for each test condition as shown in Table 1.

The configuration was clean, with landing gear, flaps, and speed brakes retracted. Since aerodynamic data for the case of landing gear and flaps extended was not explicitly available, the clean configuration was retained for the study rather than having to make aerodynamic assumptions to extend the available wind tunnel data.

The stability and control derivatives do not include variations due to speed effects since the given data were for a specific Mach number, and the speed band involved is only 24.8 m/s (48.2 knots).

The study is confined to the flight regime below stall α, where variations in derivatives are essentially linear. As a result, simplifying approximations were made by writing the derivatives as linear functions of α. The equations used for the coefficients were:

$$C_L = C_{L_o} + C_{L_\alpha}\alpha + C_{L_{\delta_e}}\delta_e \tag{B-1}$$

$$C_D = C_{D_o} + C_{D_{C_L}}C_L^2 + C_{D_{\delta_r}}\delta_r^2 - C_{Y_\beta}\beta^2 \tag{B-2}$$

$$C_m = C_{m_\alpha}\alpha + C_{m_{\delta_e}}\delta_e + \frac{\bar{c}}{2V}C_{m_q}q \tag{B-3}$$

$$C_Y = C_{Y_\beta}\beta + C_{Y_{\delta_r}}\delta_r + C_{Y_{\delta_a}}\delta_a \tag{B-4}$$

$$C_{\ell} = C_{\ell_\beta}\beta + C_{\ell_{\delta_r}}\delta_r + C_{\ell_{\delta_a}}\delta_a + \frac{b}{2V}\left(C_{\ell_p}p + C_{\ell_r}r\right) \qquad \text{(B-5)}$$

$$C_n = C_{n_\beta}\beta + C_{n_{\delta_r}}\delta_r + C_{n_{\delta_a}}\delta_a + \frac{b}{2V}\left(C_{n_p}p + C_{n_r}r\right) \qquad \text{(B-6)}$$

where (all values per radian):

$$C_{Y_{\delta_a}} = -0.0158 + 0.0615\alpha$$

$$C_{\ell_r} = 0.1 + 0.8881\alpha$$

$$C_{\ell_{\delta_r}} = 0.0115 - 0.0327\alpha$$

$$C_{\ell_{\delta_a}} = 0.058 - 0.1047\alpha$$

$$C_{n_\beta} = 0.165 - 0.525\alpha$$

$$C_{n_p} = -0.286\alpha$$

$$C_{n_{\delta_a}} = 0.00573 - 0.0274\alpha$$

All other derivatives are constant, with the following values:

$C_{L_\alpha} = 3.466$ $\qquad$ $C_{m_q} = -10.6$

$C_{L_{\delta_e}} = 0.544$ $\qquad$ $C_{Y_\beta} = -0.91$

$C_{D_{C_L}} = 0.337$ $\qquad$ $C_{Y_{\delta_r}} = 0.174$

$C_{D_{\delta_r}} = 0.088$ $\quad$ $C_{\ell_\beta} = -0.129$

$C_{m_\alpha} = -0.347$ $\quad$ $C_{\ell_p} = -0.272$

$C_{m_{\delta_e}} = -0.693$ $\quad$ $C_{n_{\delta_r}} = -0.084$

$C_{n_r} = -0.43$

The values of C_L and C_D for $\alpha = 0$ are:

$C_{L_o} = 0.025$ $\quad$ $C_{D_o} = 0.0175$

The control deflection limits are:

$\delta_e = -35, +15$ degrees

$\delta_a = 20$ degrees

$\delta_r = 30$ degrees

$\delta_v = 5.7$ degrees

$T = 67500$ N per engine

APPENDIX C

DESCRIPTION OF EXPERIMENTAL FACILITIES

The hybrid computer used in this study belongs to the NASA Langley Research Center's Aerospace Controls Research Laboratory. It is an Electronic Associates, Inc., (EAI) model, incorporating a Pacer 100 Digital Processor with 32,000 sixteen-bit words of core memory, a 681 Parallel Analog Processor, and a single fixed-head disc storage unit capable of storing 360,448 sixteen-bit words (Ref. 8). The Pacer 100 memory cycle time is 1.0 microsecond, with a subtract or divide execution time requiring 2.0 or 6.6 microseconds, respectively. Peripheral Input/Output (I/O) devices include: INPUT - Paper tape, cassette magnetic tape, cards, and interactive terminal; OUTPUT - Paper tape, cassette tape, line printer, interactive terminal, X-Y plotter, and eight-channel strip chart recorders. See Figure 5. The sixteen bit I/O Bus allows communication with the Pacer 100 at over 555,000 words per second. The system uses a Real-Time Clock Unit, initialized from the I/O Bus, to synchronize program operation between the Digital Processor and Parallel Analog Processor. The Parallel Analog Processor was used to program the nonlinear equations of motion for three of the six degrees of freedom (angular displacements), and the Pacer 100 Digital Processor was used to calculate the remaining three degrees of freedom (linear displacements) as well as to set the analog potentiometers that acted as coefficients for both the calibration checkout runs and the real-time

data gathering runs. In addition, the Digital Processor was used to implement engine dynamic characteristics, thrust vectoring logic, and AFCS logic for inner-loop stability augmentation and outer-loop autopilot functions. The simulation proceeded through the steps outlined below and shown in the simplified flow chart of Figure 6. First, aircraft physical characteristics and aerodynamic stability and control derivatives (obtained from NASA for a representative Mach 2 twin engine fighter) were read into Digital Processor storage arrays from a punched paper tape. Test point parameters and initial conditions (ICs), which could be varied, were also read into storage arrays at the same time. Then, the Digital Processor used the appropriate array values to set the variable potentiometers of the 681 Parallel Analog Processor. Calibration checks were then accomplished for a known operating trim point. If the calibration checks were passed, the main operating program was loaded into the Digital Processor from punched cards, which simultaneously activated the analog hardware and the repetitive digital loop. Once the Parallel Analog Processor was activated from the initial conditions, it operated on the aircraft equations of motion dealing with angular displacements and angular rates, at a speed of 12 million Equivalent Operations Per Second, which is significantly faster than the Digital Processor's speed of 300,000 operations per second (based on the Gibson mix of fixed-point/floating point arithmetic and logic operations). Equivalent Operations Per Second represents the speed of a digital computer that would perform the same computations in the same

time and with the same accuracy (to three decimal places in this case) as the analog computer.

At fixed time intervals dictated by the digital controlling program, selected variables from the analog side were sampled, converted to digital format, and input to the Digital Processor to be used in digital calculations. The digital Central Processor Unit (CPU) had to handle three jobs during program operations: (1) direct the overall program in terms of sampling analog channels at appropriate times, outputting digital signals to be converted to analog format at correct times, and updating aerodynamic coefficients; (2) process the linear displacement equations, which required analog inputs; and (3) process the control laws. Four basic tasks were accomplished in the Control Laws subroutine: modeling engine dynamics in terms of thrust limits and time responses; modeling Thrust Vector Control (TVC) logic in terms of delay times and rate of vectoring; SAS calculations; and Autopilot calculations. Analog inputs were needed for the last two tasks.

Once the Control Laws subroutine was completed and appropriate control inputs had been computed, these inputs were converted from digital format to analog where necessary, and then fed back to the digital or analog processor to form the closed loop system. Two eight-channel analog strip chart recorders were used to graph the control deflections and longitudinal and lateral variables as functions of real operating time.

The digital CPU scheduled the three jobs mentioned previously by using a Priority Interrupt system that gave the Control Laws subroutine

the highest priority, and made the CPU available to process the control laws every 40 milliseconds. Second priority was given to processing the linear displacement equations, which occurred every 100 ms, and the remaining time was left for overall program execution. This prioritizing prevented a situation where the control laws would be left with too little time to complete necessary calculations, which could lead to system stability problems. With the control laws given first priority, any saturation occurring in that portion of the loop would stop the program and alert the experimenter to the problem.
As functions were added to the Control Laws subroutine, an oscilloscope was used to check the time being taken for the subroutine calculations, to insure that limits were not being approached. In its final form, the Control Laws subroutine required approximately 10 milliseconds for completion.

BIBLIOGRAPHY

1. Flying Qualities of Piloted Airplanes. Military Specification MIL-F-8785B(ASG), 1969.

2. Kooy, J. M. J., and Uytenbogaart, J. W. H.: Ballistics of the Future. McGraw-Hill Book Company, Inc., 1946.

3. White, S. N.: Feasibility Study for Integrating Thrust Vectoring as Primary Flight Control System. NASA CR-165758, 1981.

4. La Froth, R. E.: Thrust Vectoring to Eliminate the Vertical Stabilizer. M.S. Thesis, Air Force Institute of Technology, 1979.

5. Craig, A.: Flying Sideways during Landing Maneuvers. Atmospheric Flight Mechanics Conference, Palo Alto and Moffett Field, CA. 11-13 Sep 1972.

6. Etkin, Bernard: Dynamics of Atmospheric Flight. Wiley and Sons, Inc., NY, 1972.

7. Lacey, David W., and Murphy, Richard D.: Jet Engine Thrust Turning by the Use of Small Externally Mounted Vanes. David W. Taylor Naval Ship Research and Development Center Report 82/080, 1982.

8. EAI Pacer Scientific and Engineering Computer Systems Handbook. EAI, Inc., 1972.

TABLE 1. - CHARACTERISTICS AND PARAMETERS FOR EACH FLIGHT CONDITION TESTED

	Condition 1	Condition 2	Condition 3	Condition 4
Weight, W, N (lb)	159 652(35 891)	201 950(45 400)	201 950(45 400)	150 350(33 800)
I_X, kg-m^2	34 574	43 734	43 734	32 560
I_Y	225 900	285 750	285 750	212 738
I_Z	253 540	320 713	320 713	238 768
I_{XZ}	-13 558	-17 150	-17 150	-12 768
α_o, deg	10	15	17.5	17.5
Mass, m, kg	16 280	20 593	20 593	15 332
C_L	.58	.86	1.00	1.00
C_D	.13	.27	.35	.35
Thrust, T, N (lb)	35 262(7 927)	59 880(13 462)	67 484(15 171)	50 241(11 295)
Altitude, h, m	sea level	sea level	sea level	sea level
V, m/s (knots)	87.27(170)	79.07(154)	72.41(141)	62.48(121.5)
$\bar{q}$, N/m^2	4 669	3 833	3 214	2 393

TABLE 2 - REQUIRED STEADY STATE CONTROL DEFLECTIONS FOR RIGHT ENGINE OUT AND $\beta = 0$

	Condition 1		Condition 2		Condition 3		Condition 4	
	Unvectored	Vectored	Unvectored	Vectored	Unvectored	Vectored	Unvectored	Vectored
Sideslip, β, deg	0	0	0	0	0	0	0	0
Bank, ϕ, deg	-1.4	-1.3	-1.9	-1.7	-2.2	-2.0	-2.2	-2.0
δ_r, deg	4.8	0	10.1	0	13.5	0	13.5	0
δ_a, deg	-0.7	0	-0.9	0	-0.7	0	-0.7	0

TABLE 3. - TEST MATRIX

	Condition 1	Condition 2	Condition 3	Condition 4
Basic Non-vectored	X[b]	X[b]	X[b]	X[b]
Vectored thrust				
Reaction delay sec / Actuation interval sec				
2 / 1	X	X	X[b]	X
2 / 1[a]	X	X	X[b]	X
2 / 2	X	X	X	X
2 / 2[a]	X	X	X	X
4 / 1	X	X	X	X
4 / 1[a]	X	X	X	X
4 / 2	X	X	X[b]	X
4 / 2[a]	X	X	X[b]	X

[a]Includes thrust command double

[b]Included in List of Figures

TABLE 4. - SIMULATION TIME HISTORY VALUES

(a) Basic non-vectored flight conditions

	Condition 1		Condition 2		Condition 3		Condition 4	
	Peak	Steady-state	Peak	Steady-state	Peak	Steady-state	Peak	Steady-state
V, m/s		87.27		79.07		72.41		62.48
α, deg	12	10	18	15	20	17.5	20	17.5
q, rad/s	-.007	0	-.01	0	.03	0	.035	0
$\dot{z}(-\dot{h})$, m/s	8.2	0	14	0	22	0	21	0
$\Delta z(-\Delta h)$, m	220	0	350	0	450	400	375	0
T, N	40 000	35 262	67 500	59 880	67 500	67 484	58 000	50 241
p, rad/s	.03	0	.085	0	.102	0	.115	0
ϕ, deg	2.6	-1.4	11.5	-1.89	-30	-2.18	-30	-2.18
r, rad/s	.02	0	.035	0	.075	0	.09	0
β, deg	-1.1	0	-2.7	0	-3.3	0	-3.0	0
δ_r, deg	5.4	4.8	11.1	10.2	14.4	13.5	16	13.5
δ_a, deg	-4.4	-0.6	-16	-.6	-20	-.6	-20	-.6
ψ, deg	4.0	2.0	17.5	5.6	48.6	5.6	64.2	5.6

TABLE 4. - Concluded.

(b) Vectored thrust steady-state values.

	Condition 1	Condition 2	Condition 3	Condition 4
ϕ, deg	-1.29	-1.72	-1.95	-1.95
β, deg	0	0	0	0
δ_r, deg	0	.15	0	0
δ_a, deg	0	0	.2	.2

TABLE 5. - EFFECT OF COMMAND DOUBLE ON VECTORED THRUST LATERAL VARIABLES

	Condition 3 2 sec reaction 1 sec actuation No command double		Condition 3 2 sec reaction 1 sec actuation Command double		Condition 3 4 sec reaction 2 sec actuation No command double		Condition 3 4 sec reaction 2 sec actuation Command double	
	Peak	Steady-state	Peak	Steady-state	Peak	Steady-state	Peak	Steady-state
p, rad/s	-0.132	0.0	-0.132	0.0	-0.132	0.0	-0.132	0.0
ϕ, deg	14.5	-2.9	14.5	-2.9	21.7	-2.9	23.6	-2.9
r, rad/s	.04	0	.04	0	.053	0	.06	0
β, deg	-3.0	0	-3.0	0	-3.2	0	-3.2	0
δ_r, deg	6.6	0	6.6	0	7.2	0	7.8	0
δ_a, deg	-17.0	.2	-18.5	.2	-20	.2	-20	.2
ψ, deg	8.6	2.9	8.6	2.9	15.7	2.9	17.5	2.9

TABLE 6. - EFFECT OF THRUST VECTORING ON LONGITUDINAL VARIABLES

	Condition 3	Condition 3	Condition 3
	Non-vectored	2 sec reaction 1 sec actuation No command double	4 sec reaction 2 sec actuation No command double
Variation in V, m/s	64.5-80.0	64.0-73.5	65.0-75.5
Maximum α, deg	20	20	20
Maximum δ_e, deg	-10.8	-10.2	-10.5
Maximum $\dot{z}$, m/s	22	15	17.75
Peak/Steady-state Δz, m	450/400	370/350	375/350
Steady-state T, N	67 484	67 484	67 484

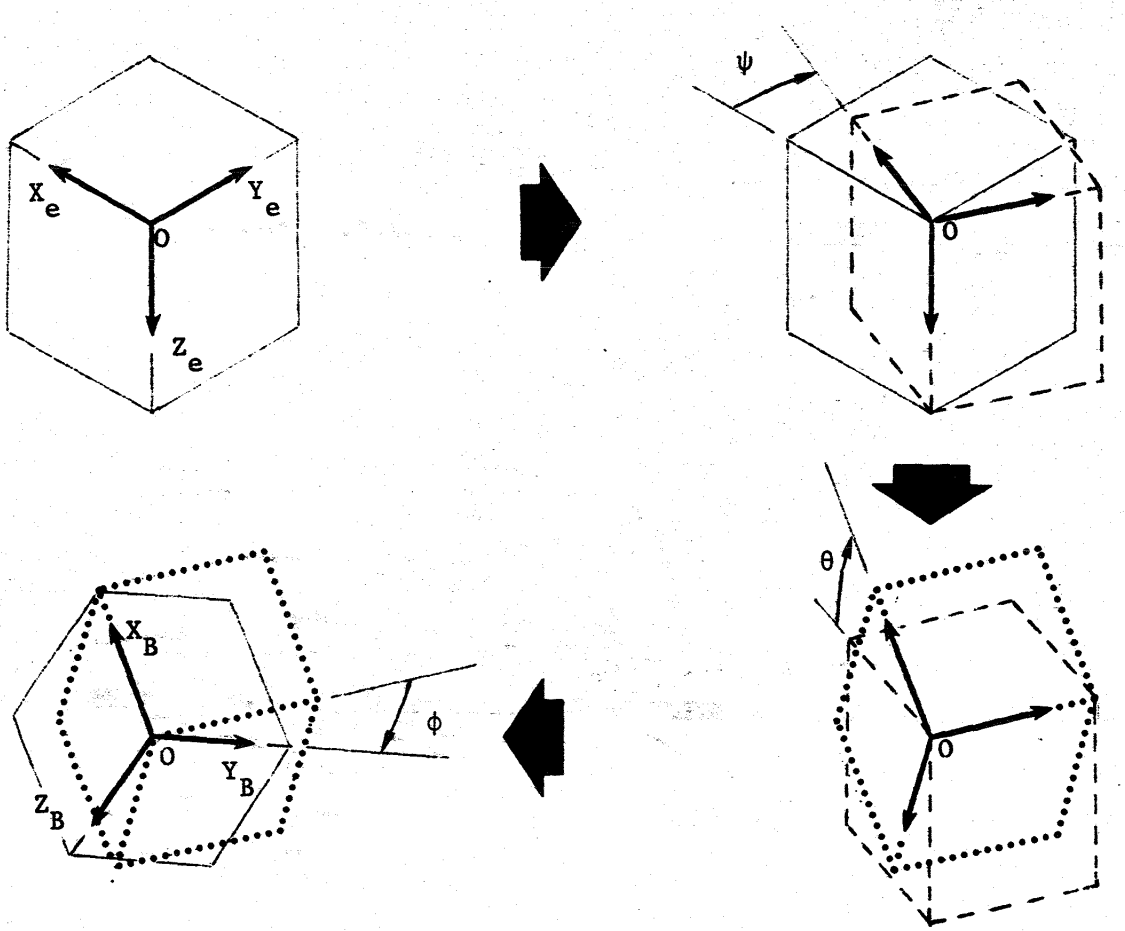

Figure 1. - Definition of Euler angles.

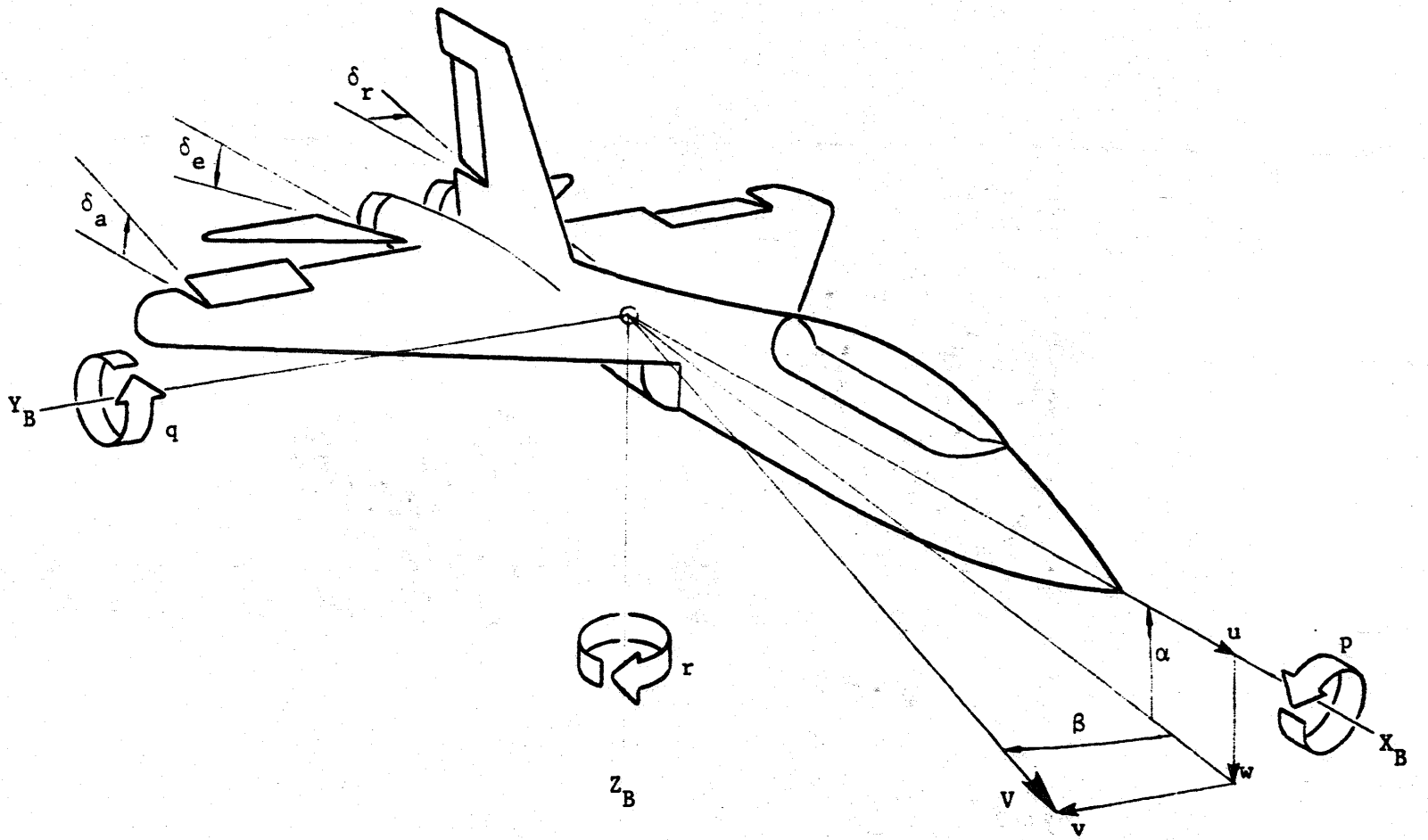

Figure 2. - Definition of body axes, control deflections, and response variables. Arrows indicate positive direction.

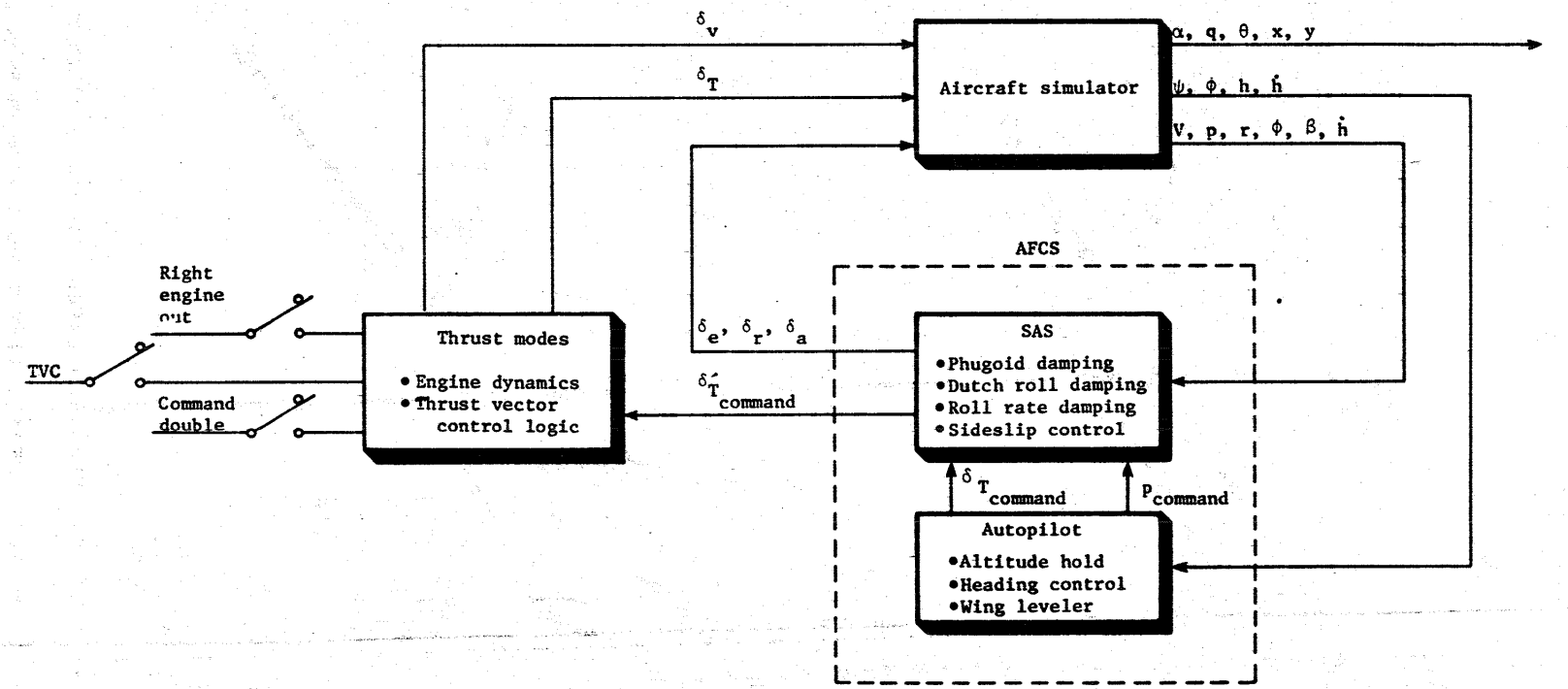

Figure 3. - Block diagram of AFCS functions.

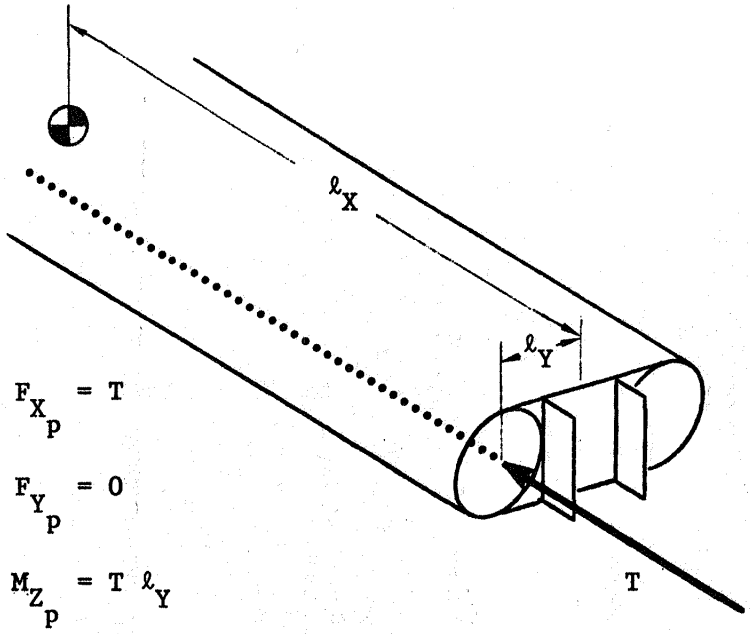

$F_{X_p} = T$

$F_{Y_p} = 0$

$M_{Z_p} = T\ \ell_Y$

(a) Right engine out with remaining thrust non-vectored.

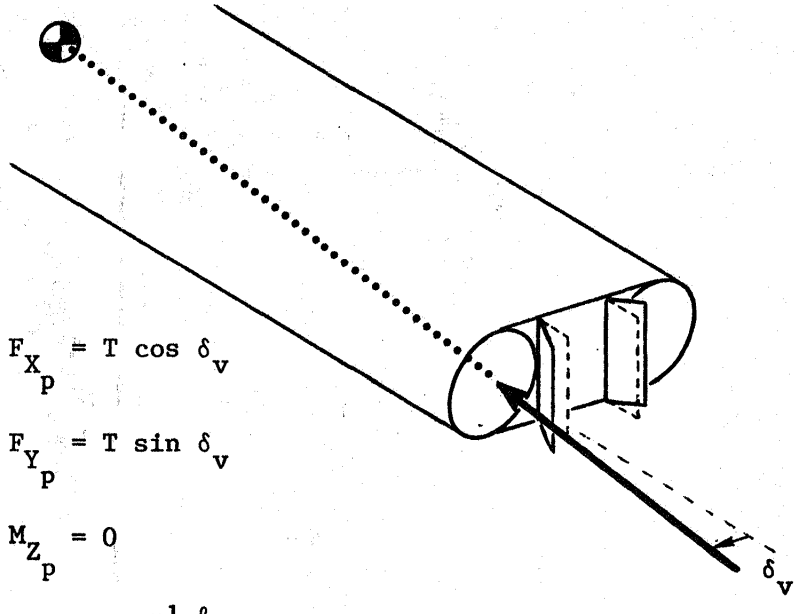

$F_{X_p} = T \cos \delta_v$

$F_{Y_p} = T \sin \delta_v$

$M_{Z_p} = 0$

$\delta_v = \tan^{-1} \frac{\ell_Y}{\ell_X}$

(b) Right engine out with remaining thrust vectored through cg.

Figure 4. - A possible lateral thrust vectoring method.

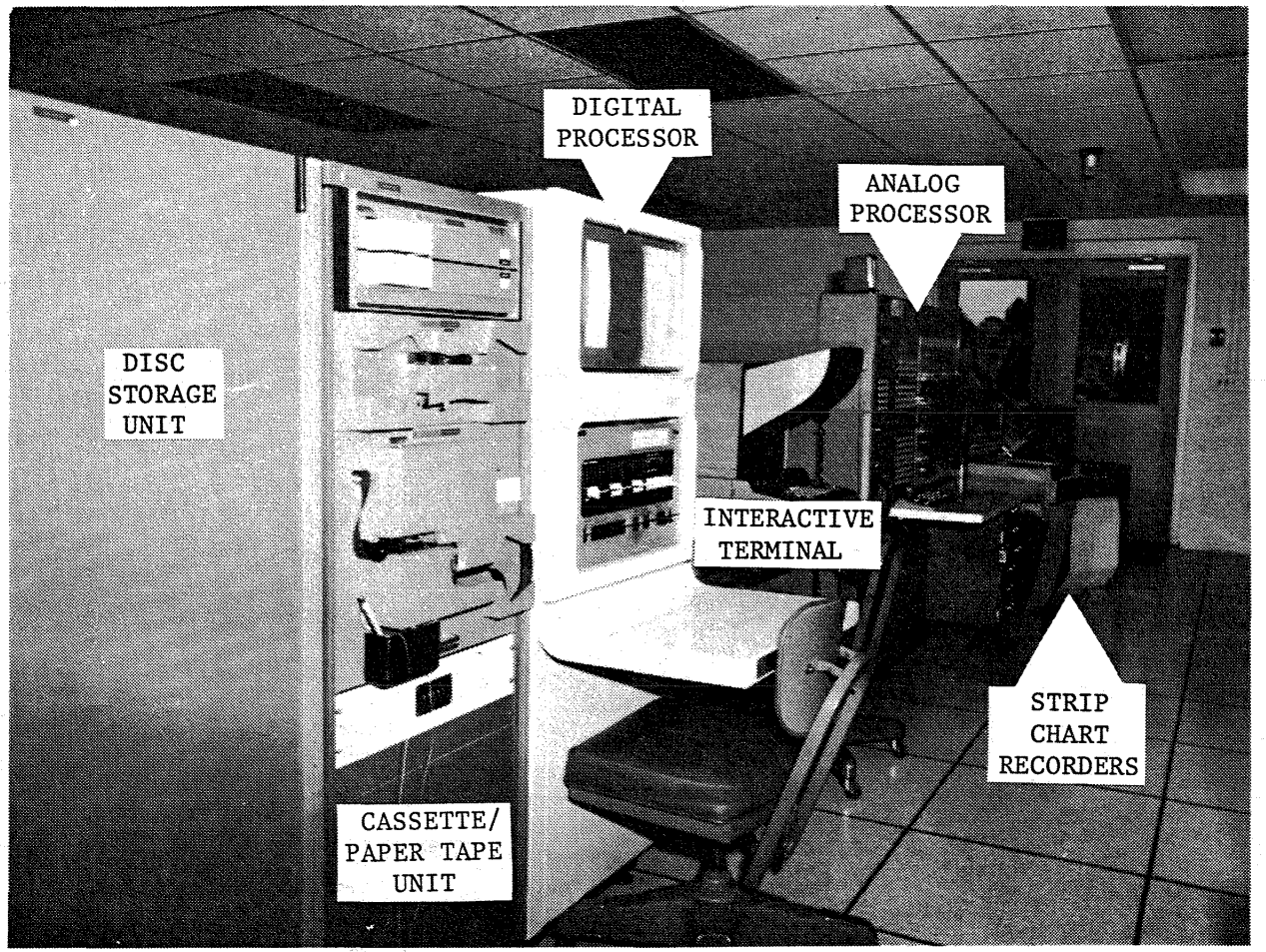

(a) Close view of digital equipment.

Figure 5. - Layout of experimental facilities.

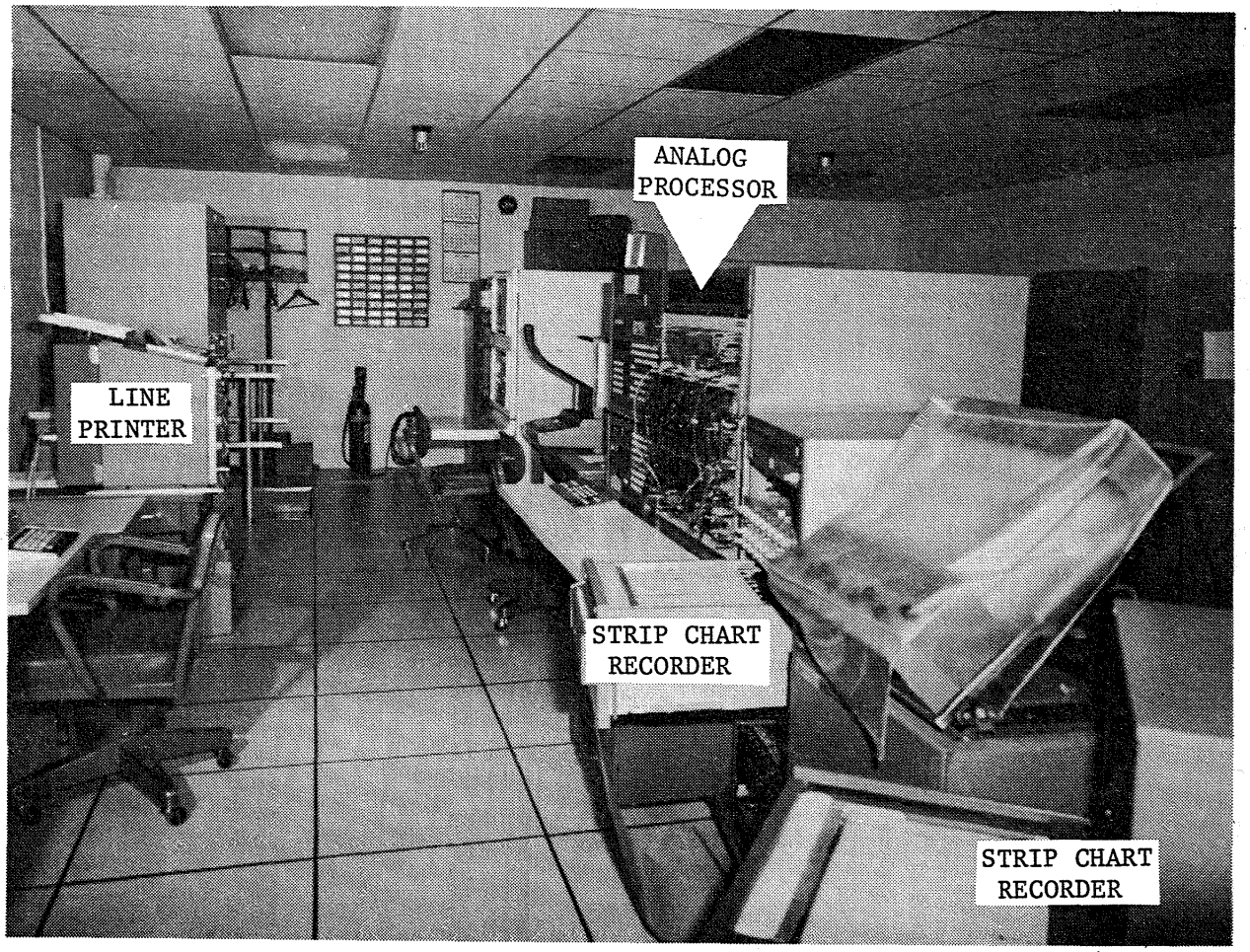

(b) Close view of analog equipment.

Figure 5. - Concluded.

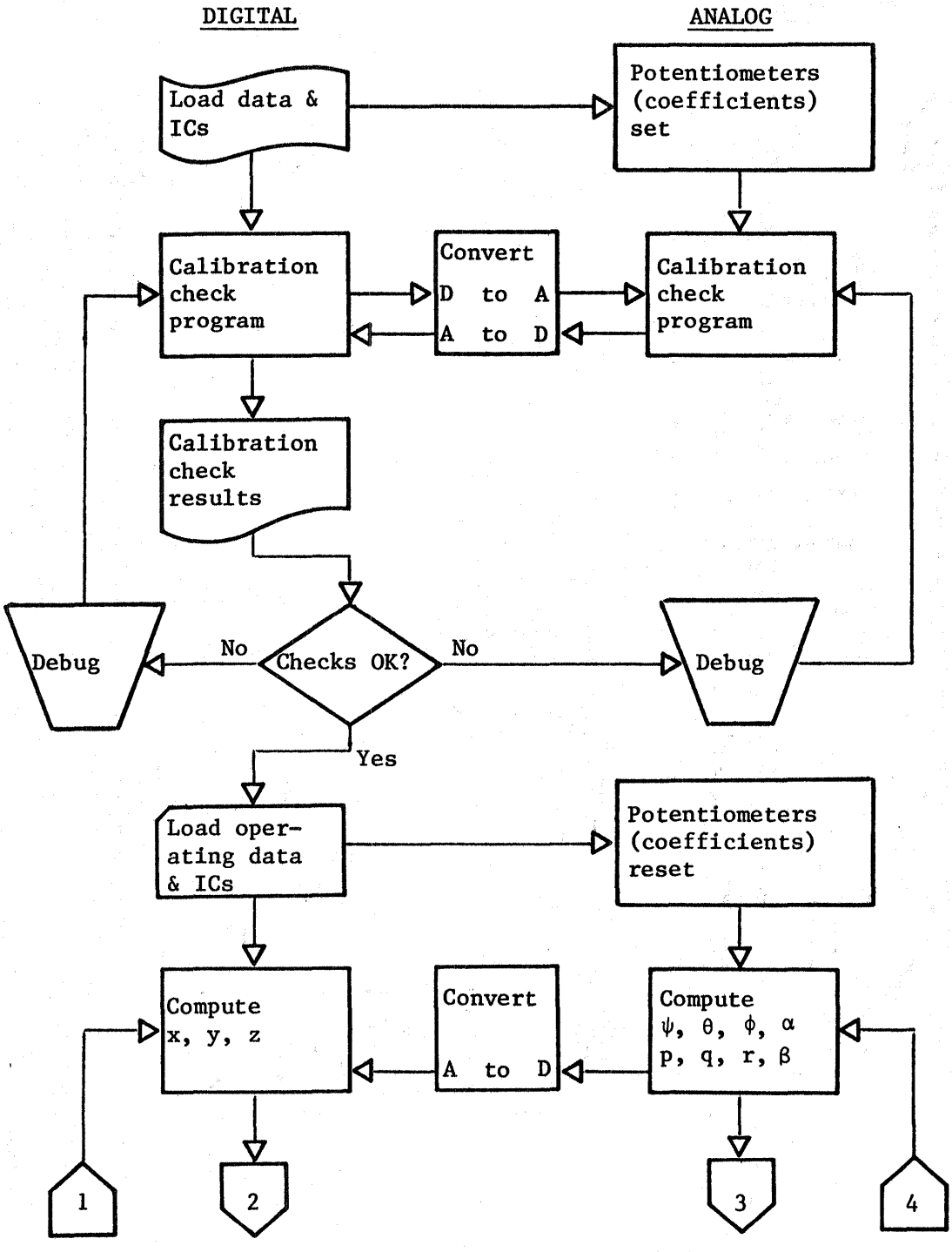

Figure 6. - Simulation flow chart.

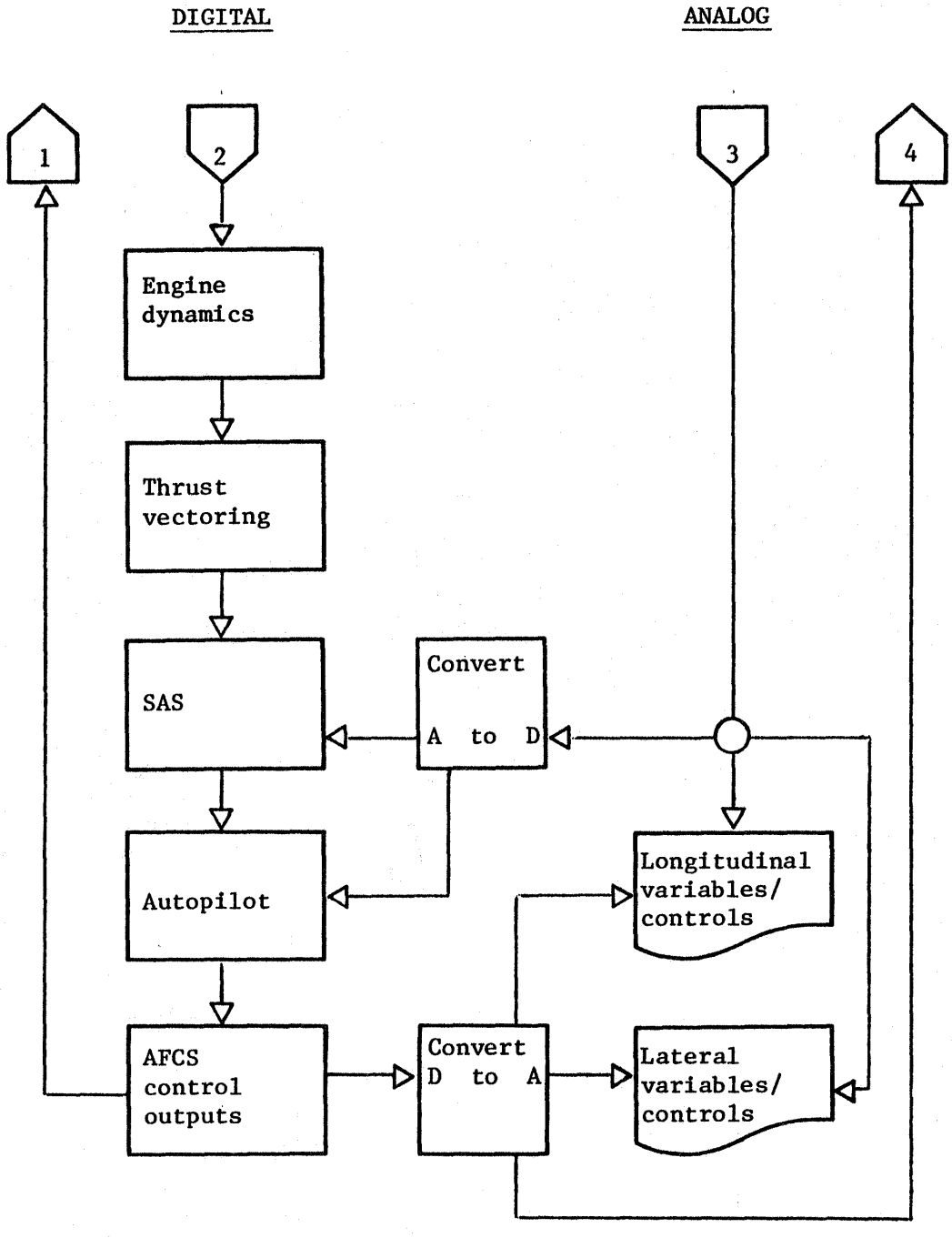

Figure 6. - Concluded.

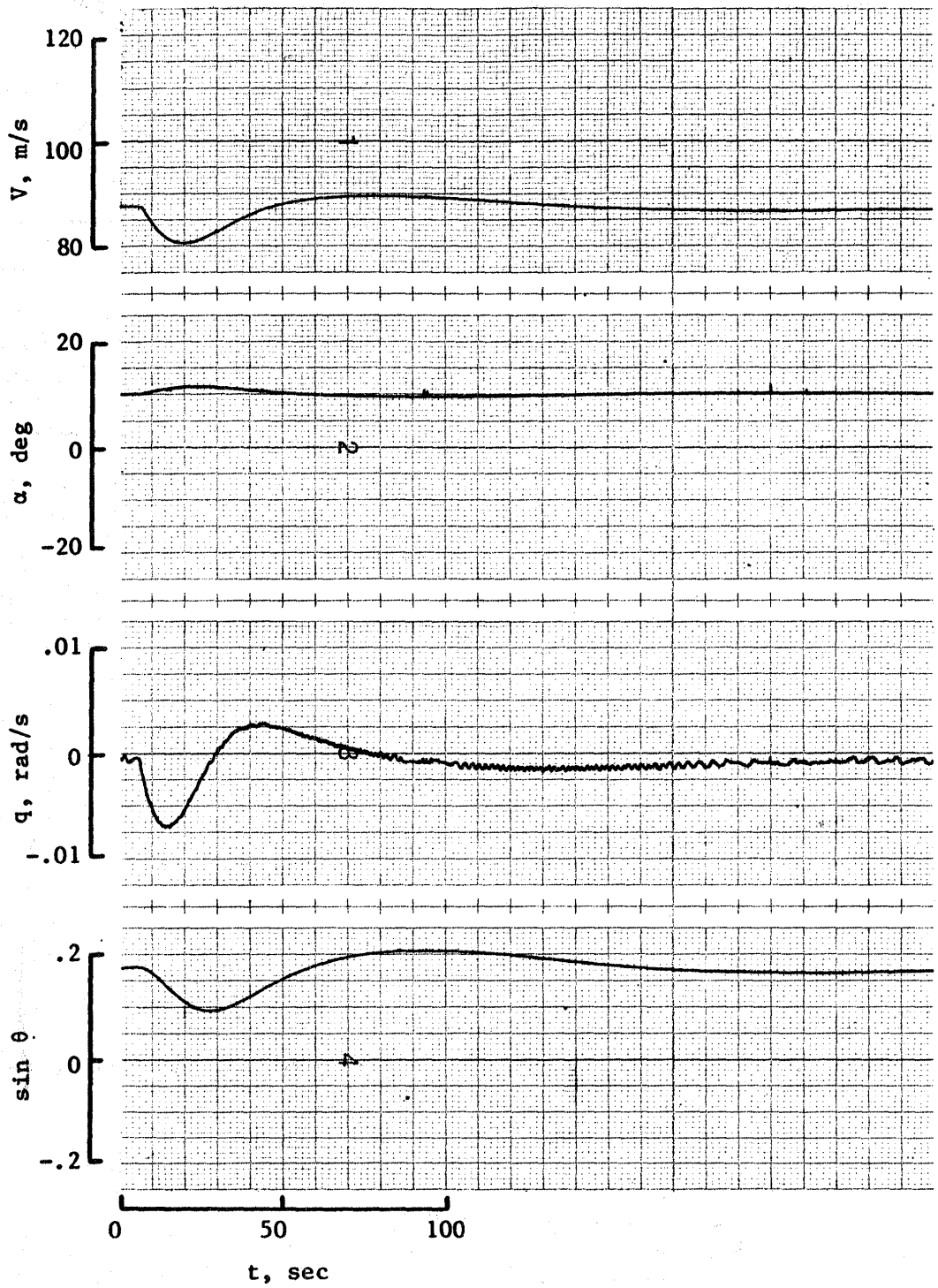

Figure 7. - Condition 1 longitudinal variables for no thrust vectoring.

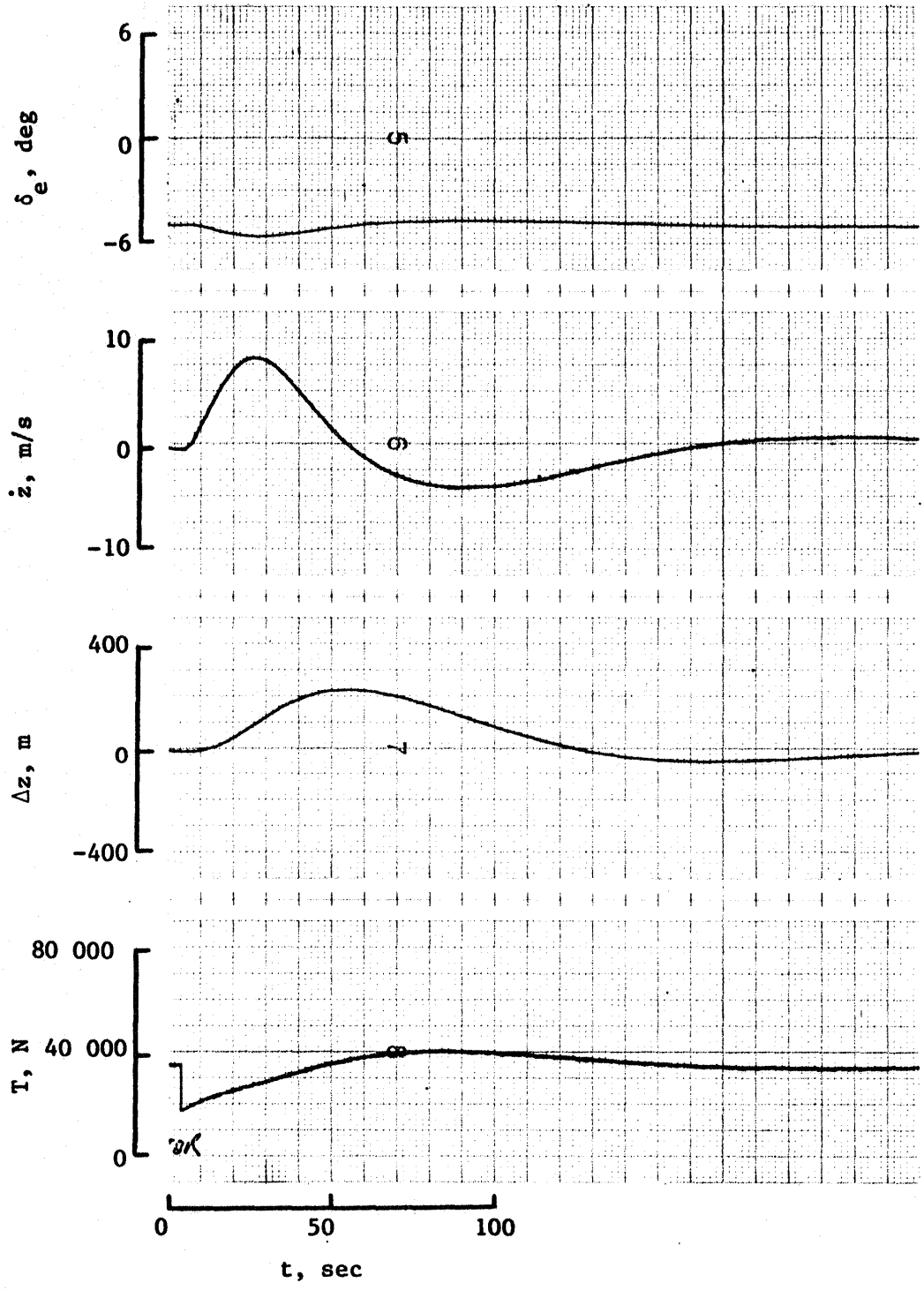

Figure 7. – Concluded.

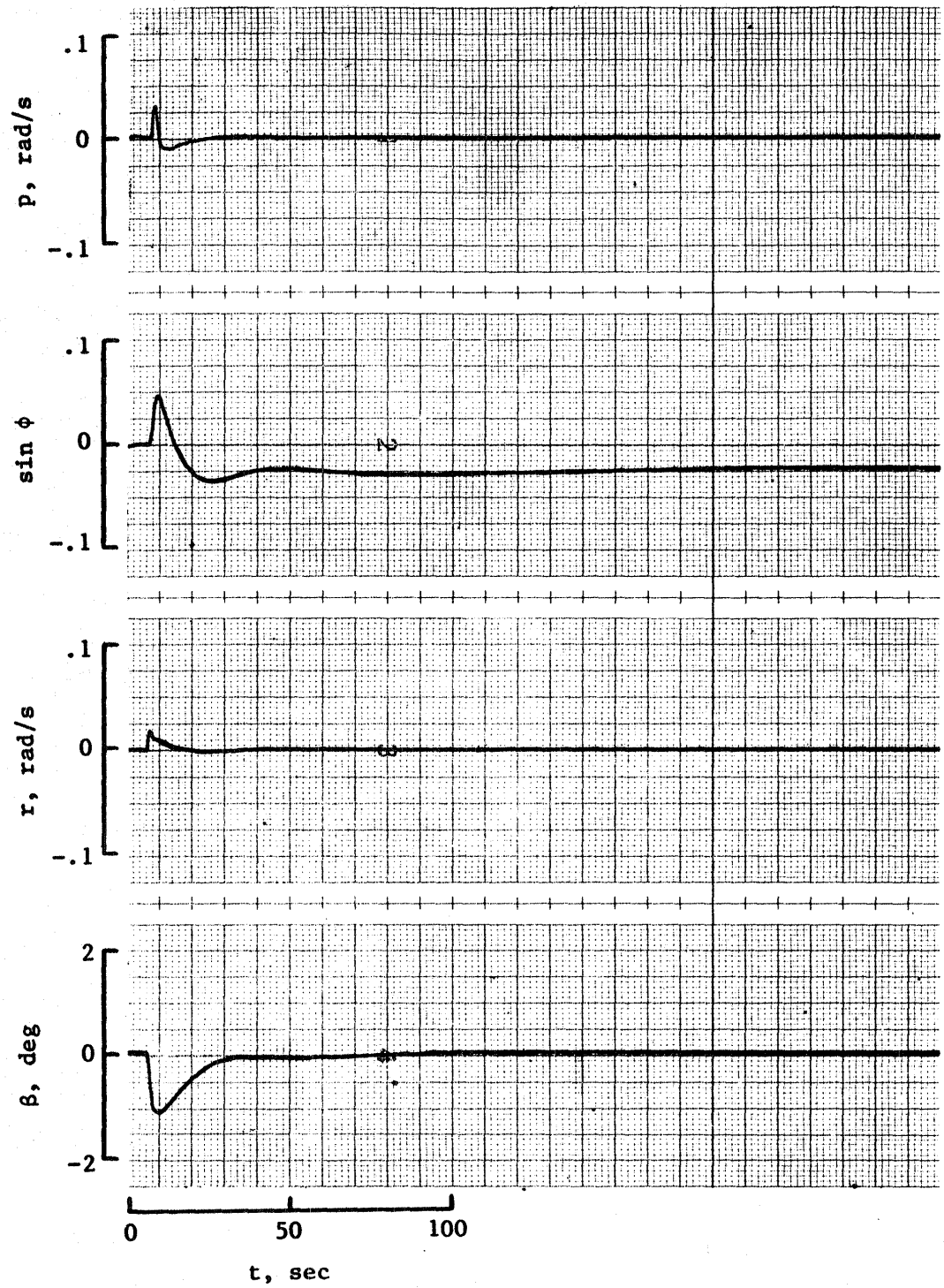

Figure 8. - Condition 1 lateral variables for no thrust vectoring.

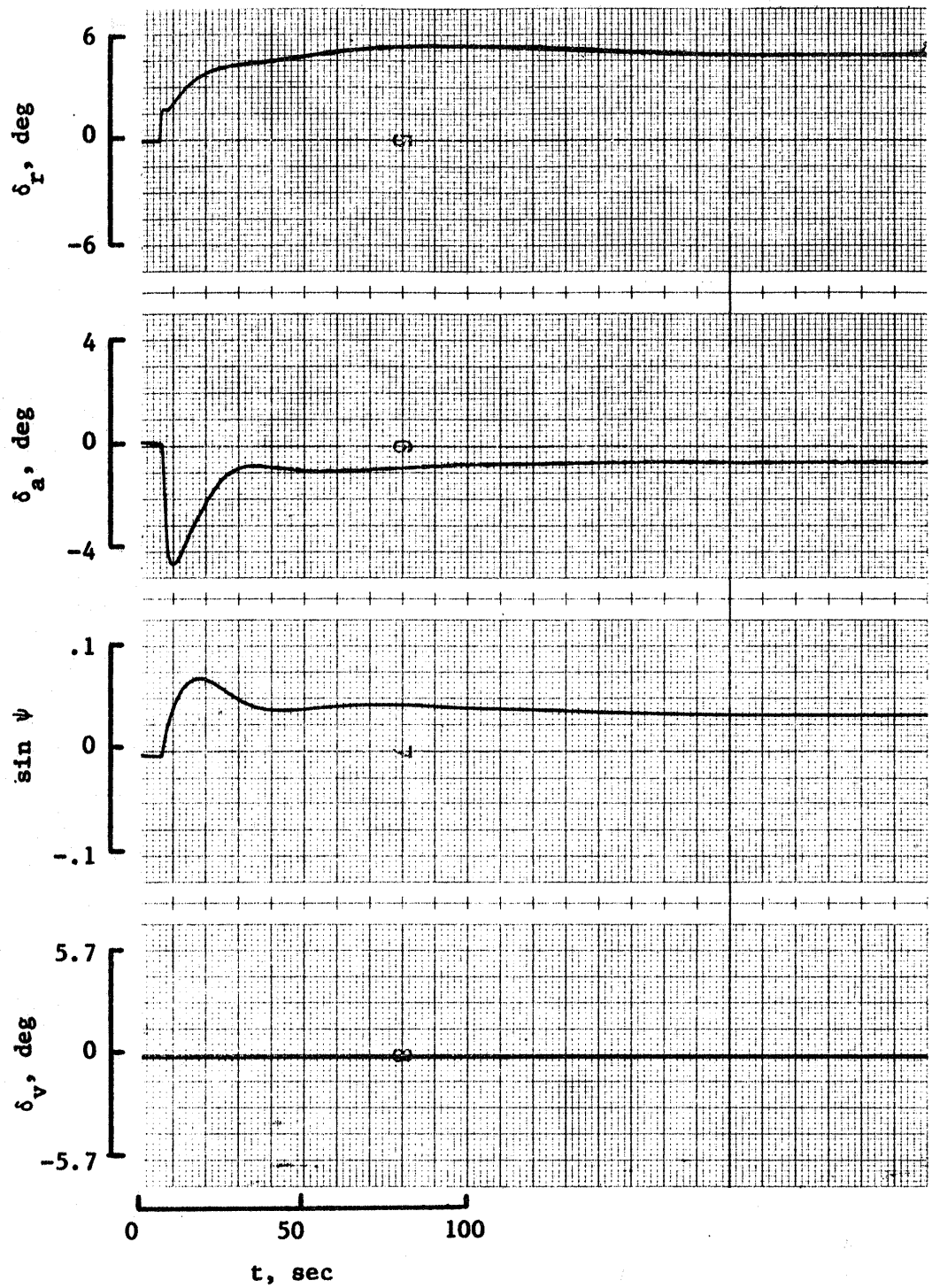

Figure 8. - Concluded.

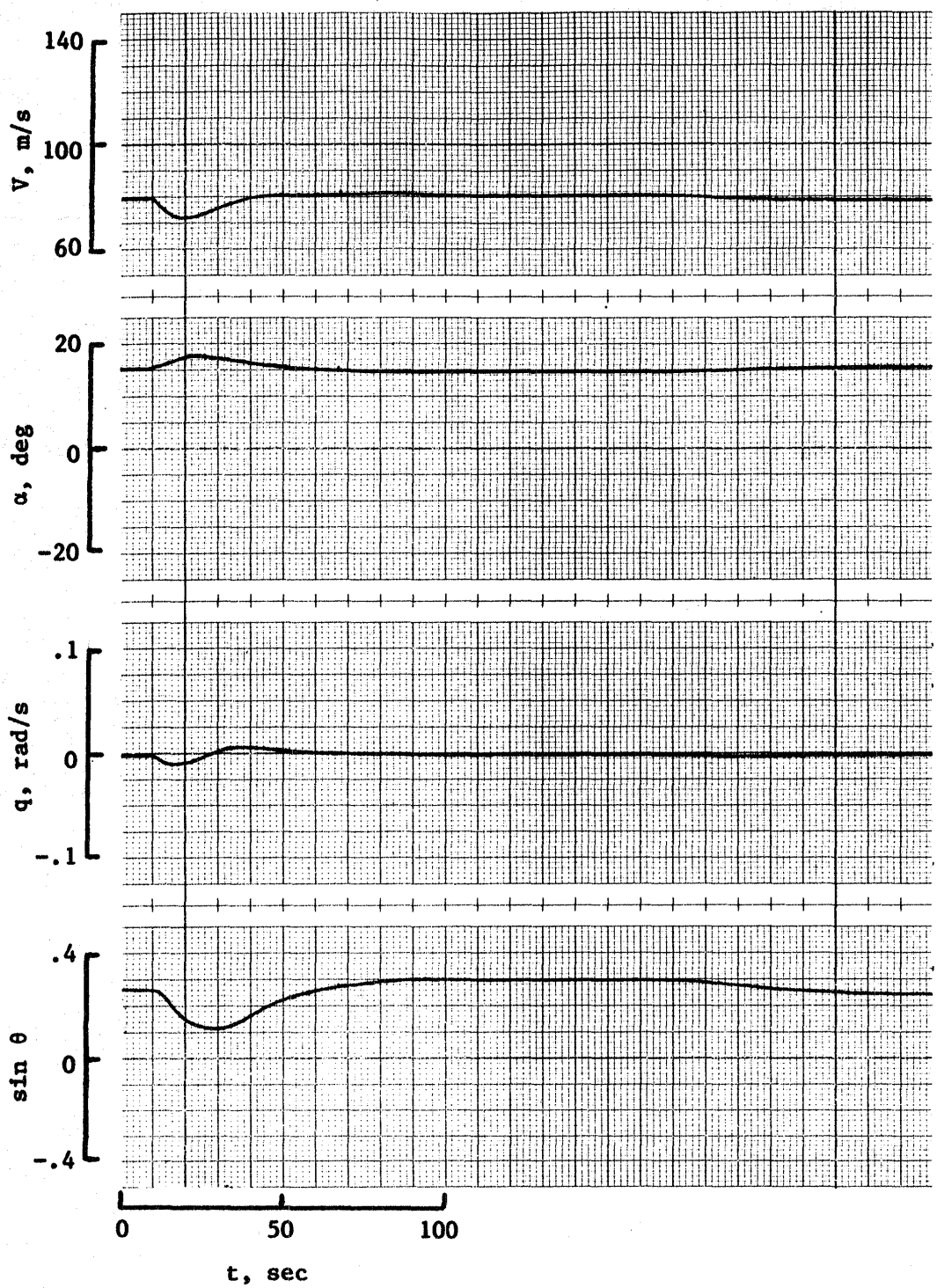

Figure 9. - Condition 2 longitudinal variables for no thrust vectoring.

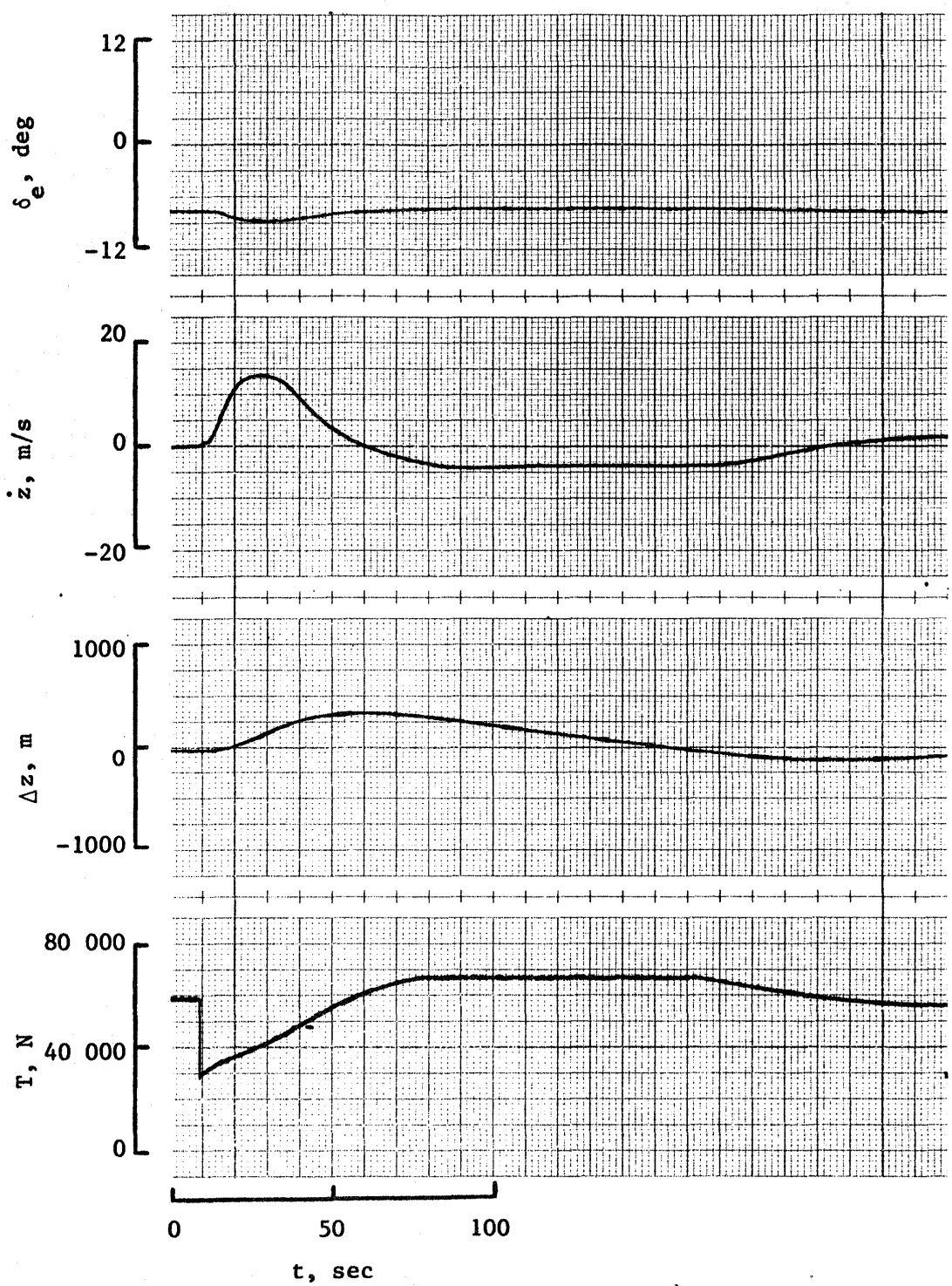

Figure 9. - Concluded.

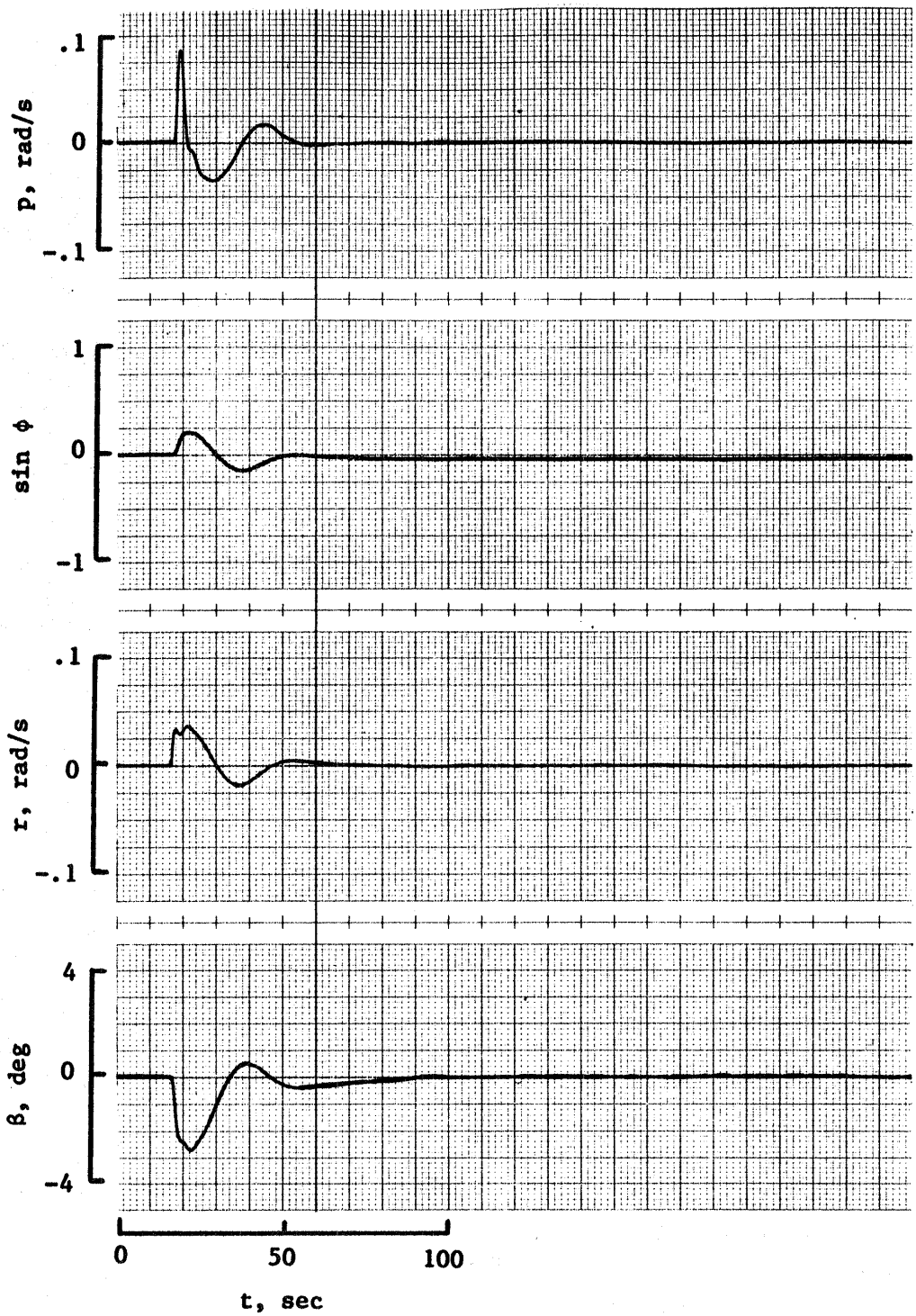

Figure 10. - Condition 2 lateral variables for no thrust vectoring.

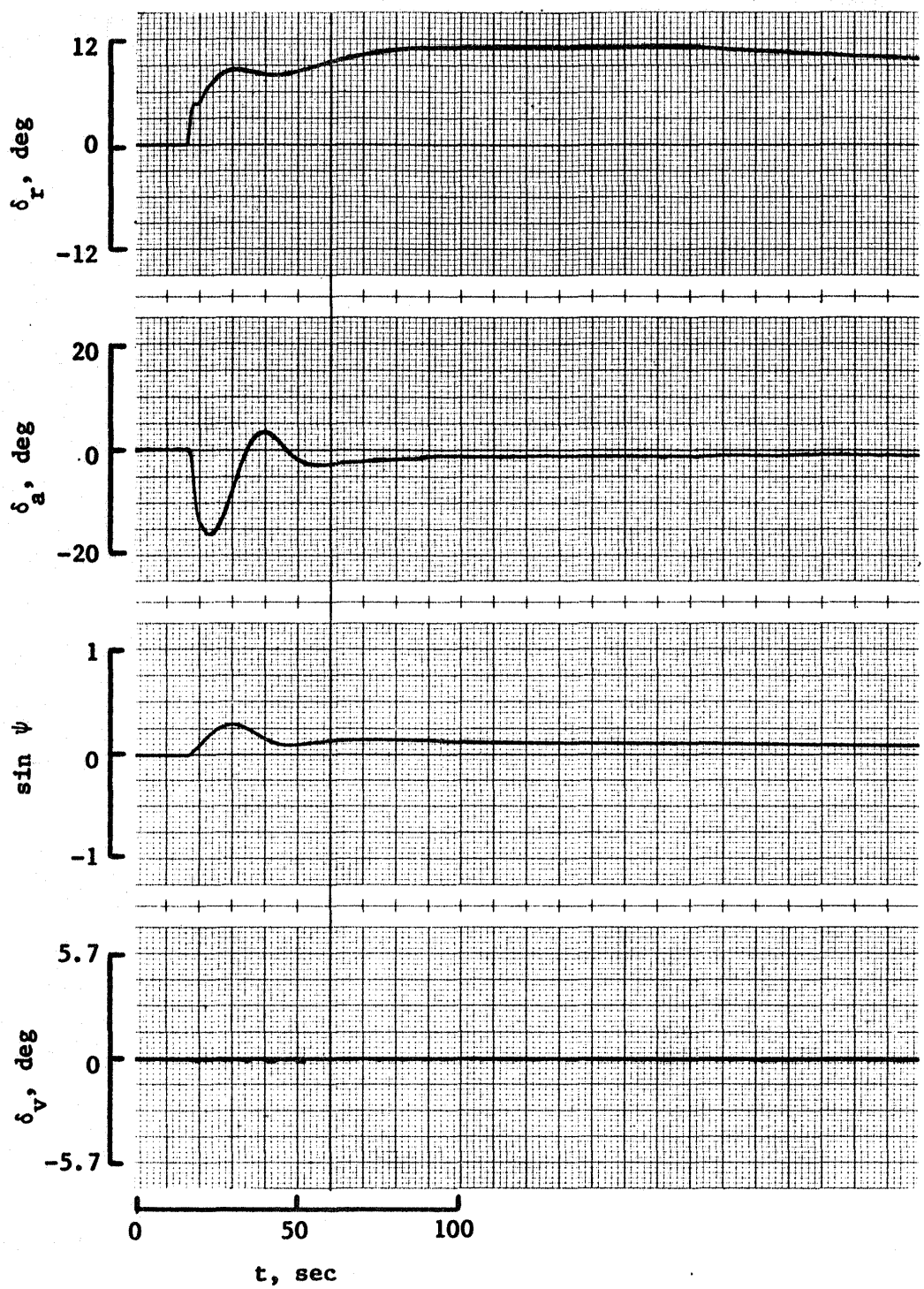

Figure 10. - Concluded.

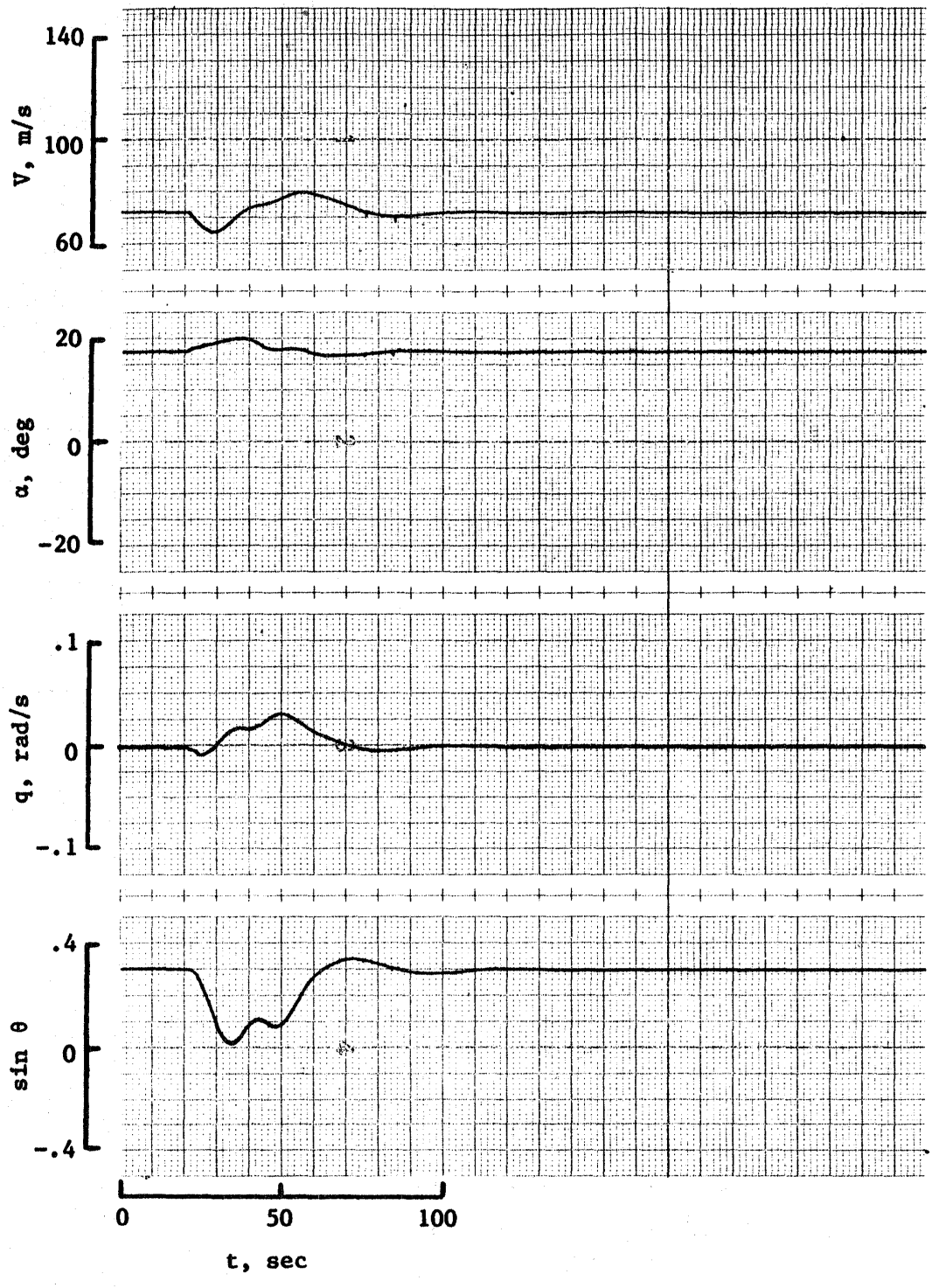

Figure 11. - Condition 3 longitudinal variables for no thrust vectoring.

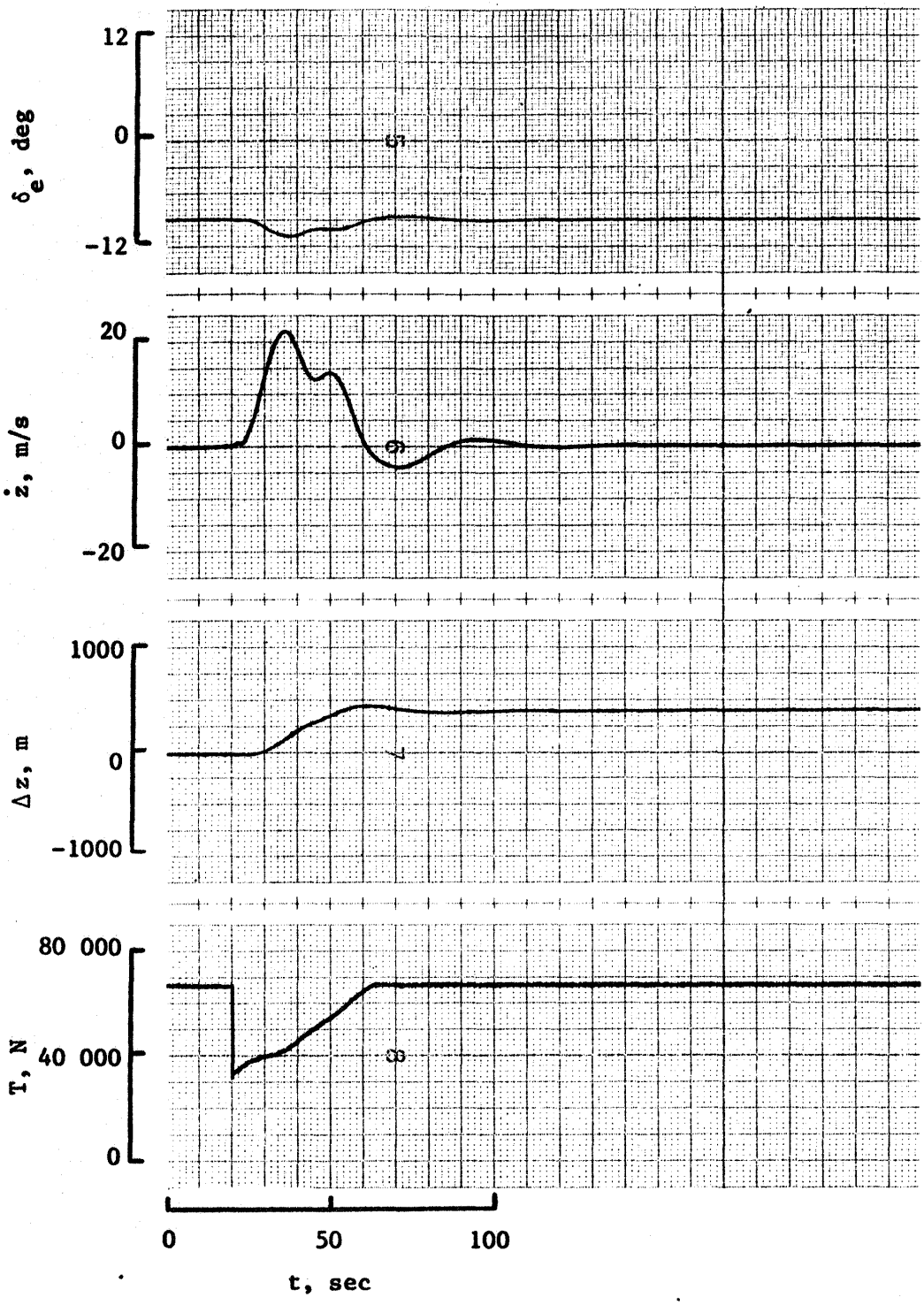

Figure 11. - Concluded.

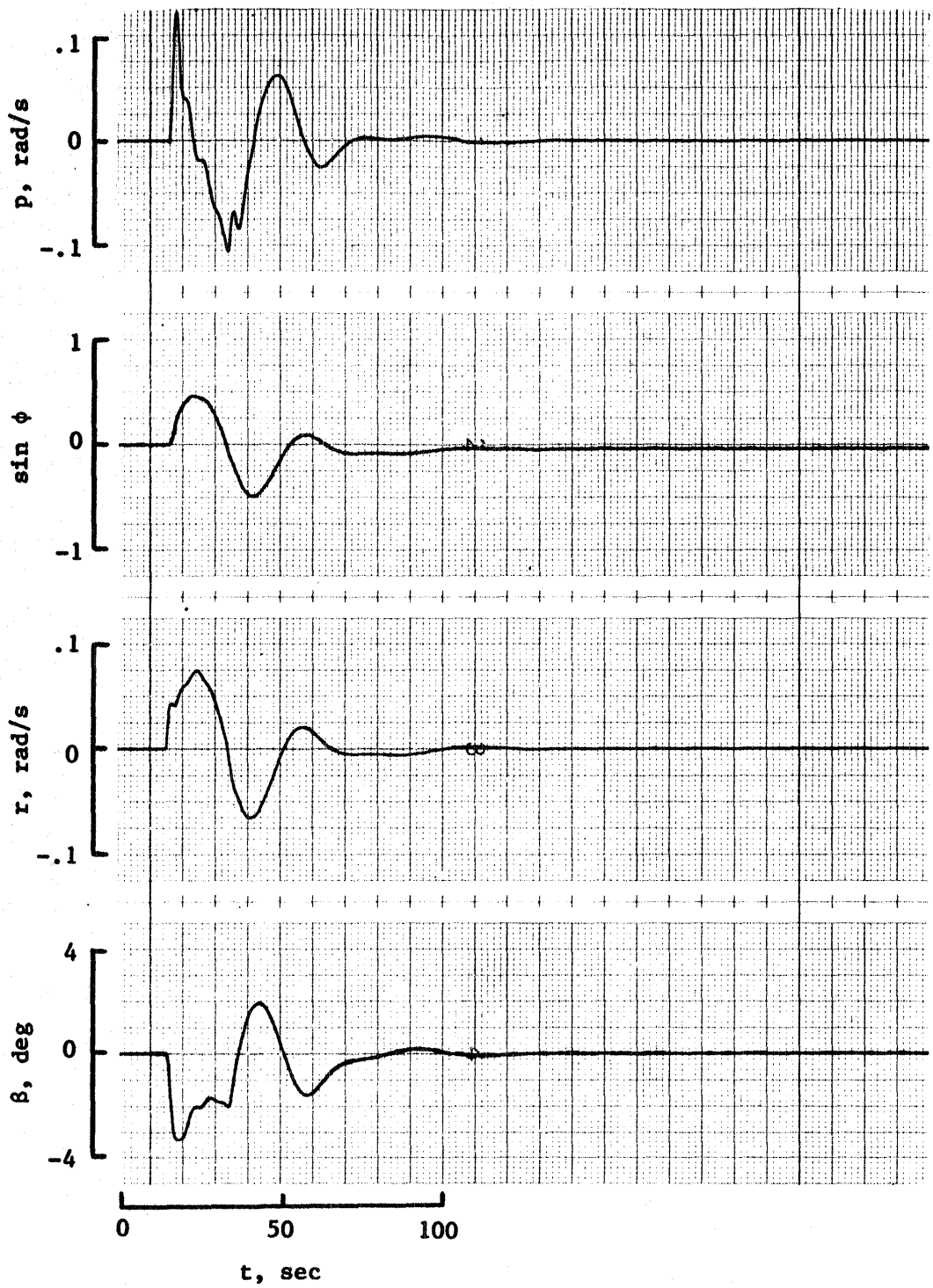

Figure 12. - Condition 3 lateral variables for no thrust vectoring.

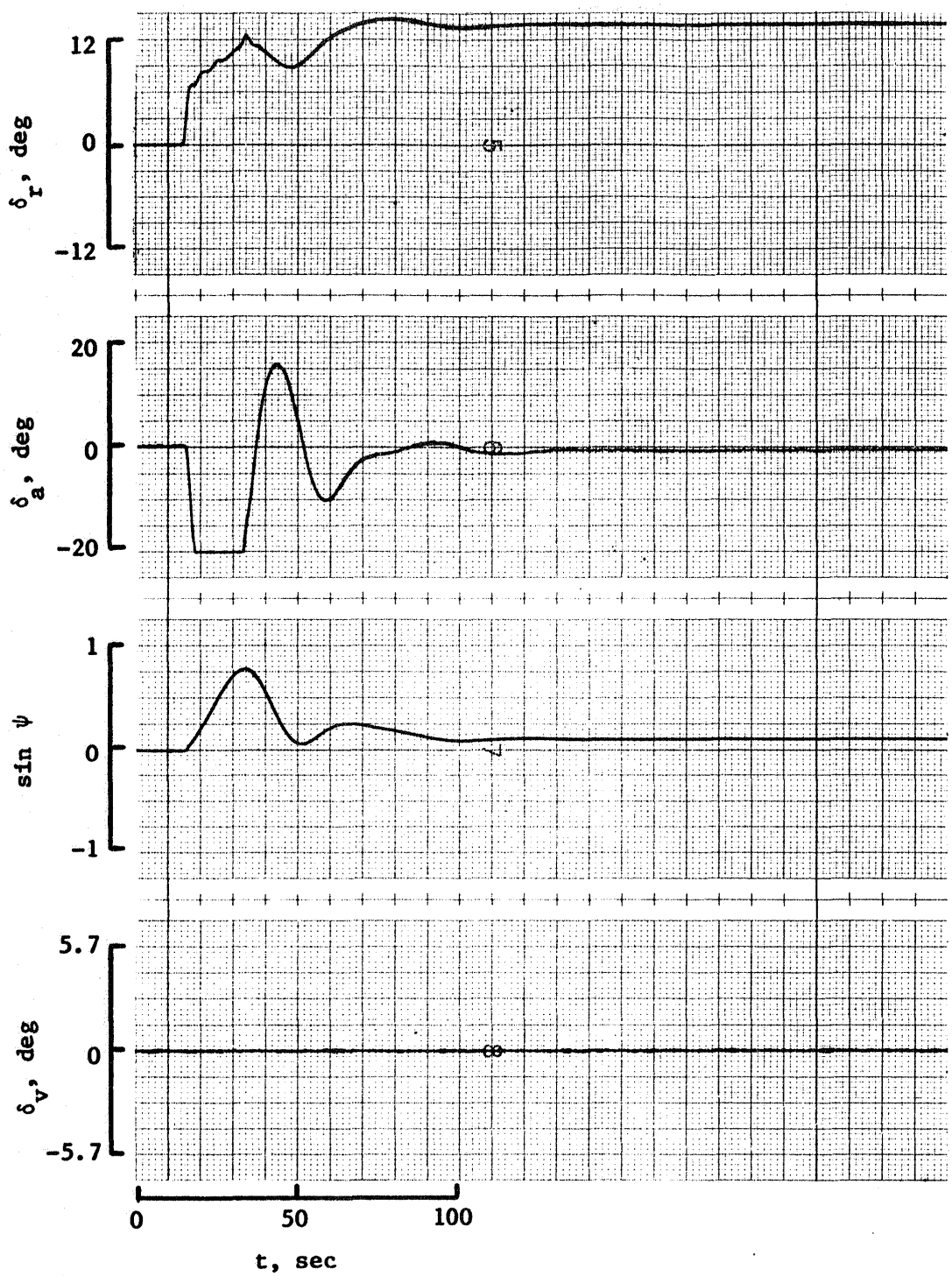

Figure 12. - Concluded.

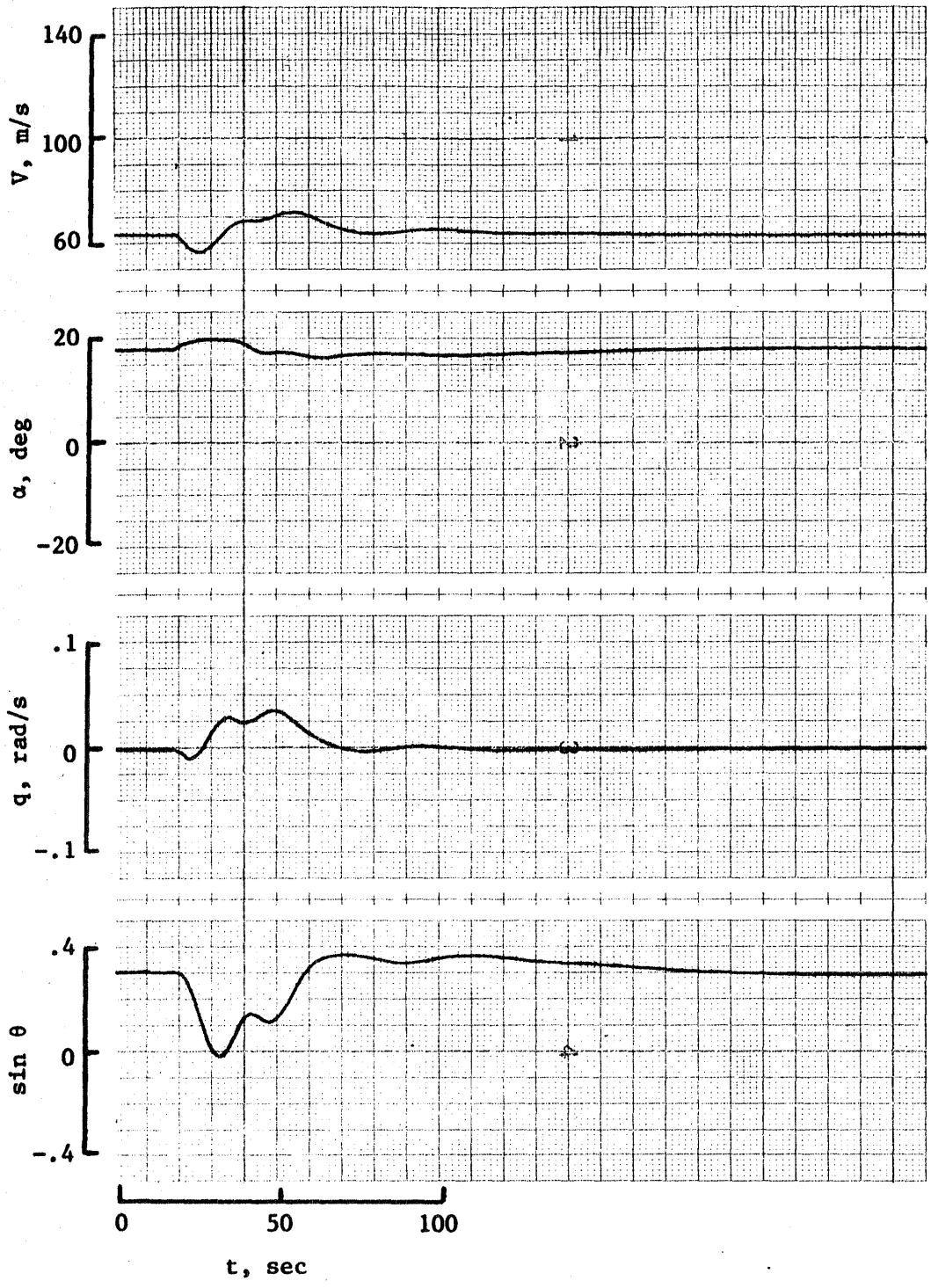

Figure 13 - Condition 4 longitudinal variables for no thrust vectoring.

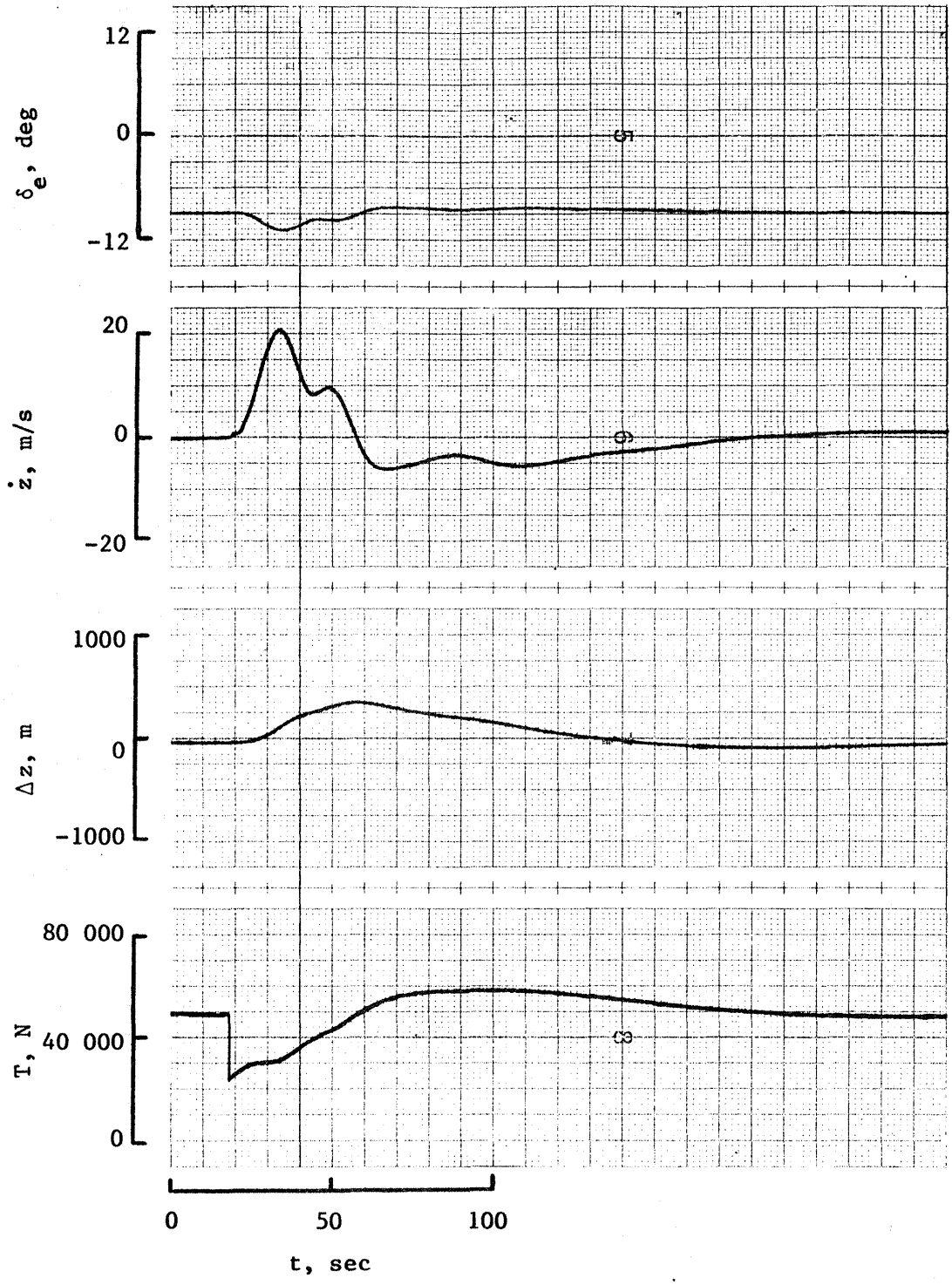

Figure 13. - Concluded.

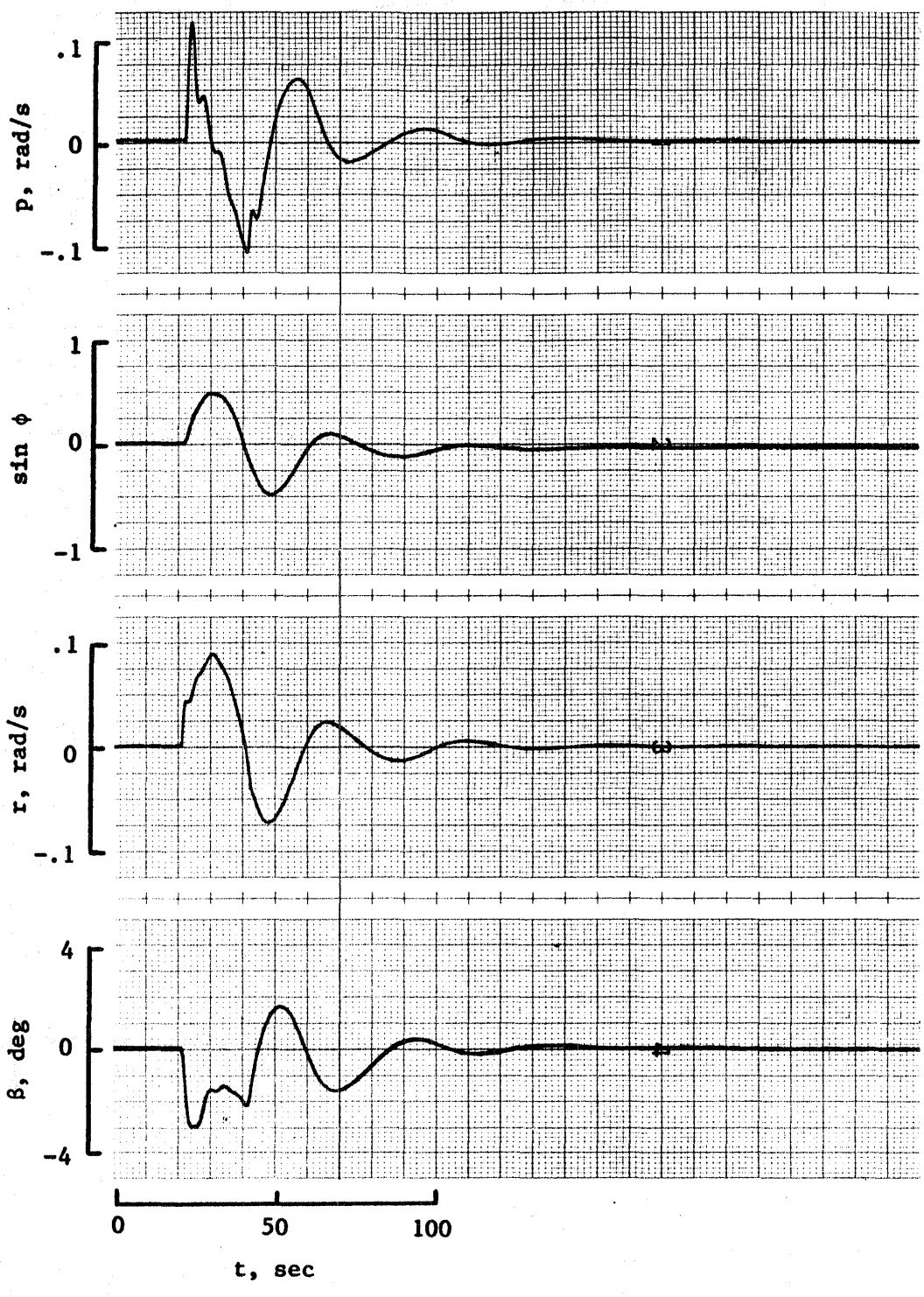

Figure 14. - Condition 4 lateral variables for no thrust vectoring.

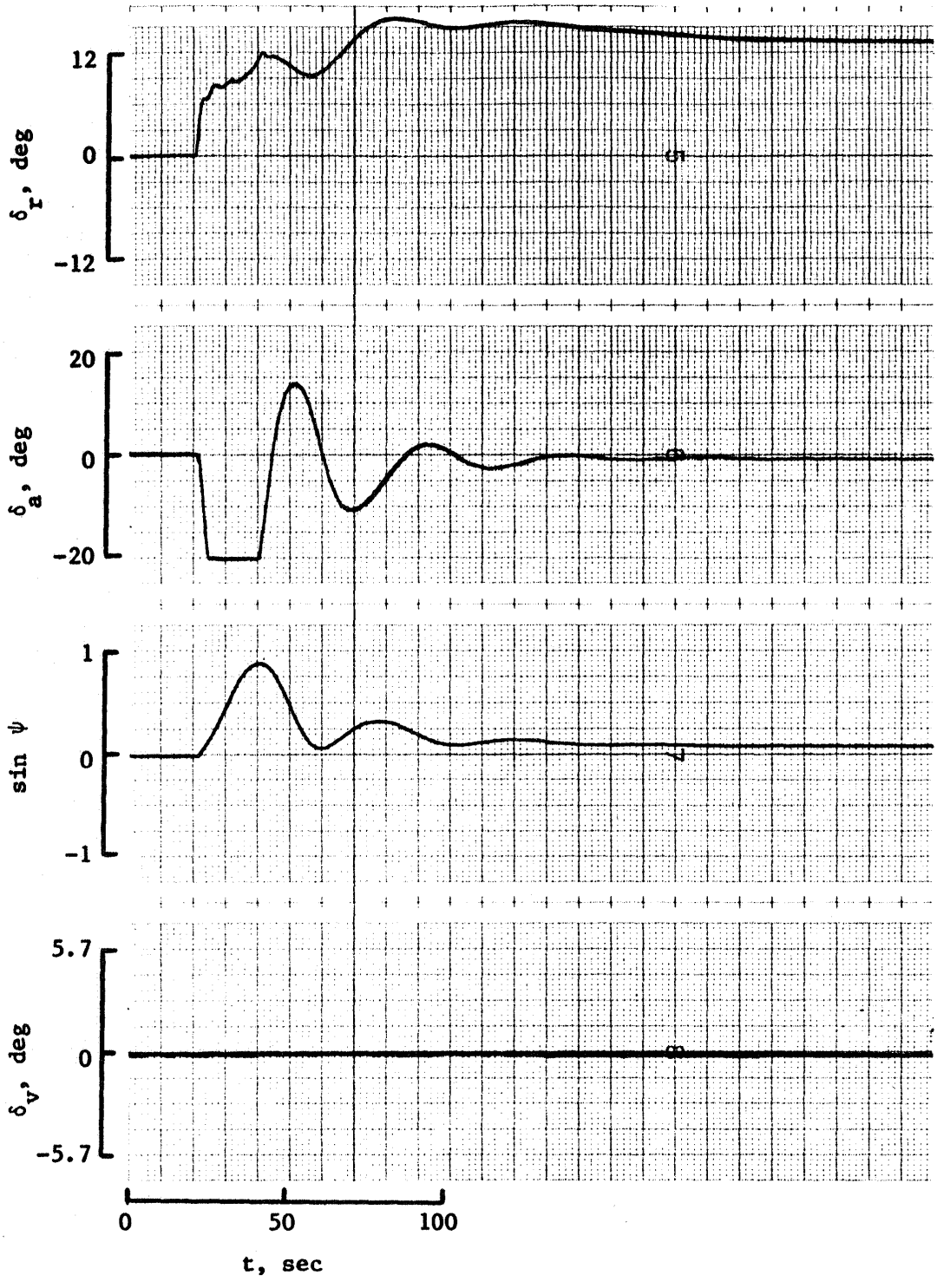

Figure 14. - Concluded.

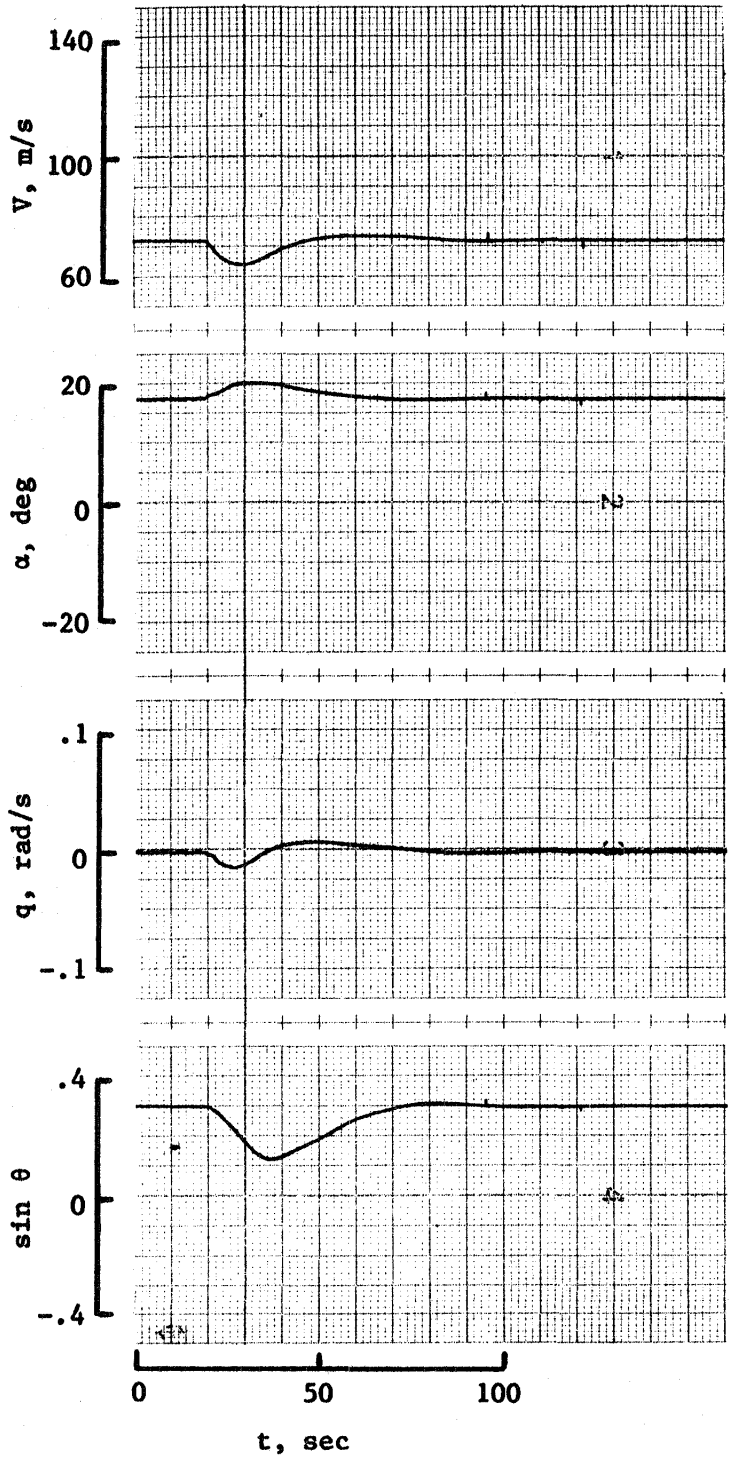

Figure 15. - Condition 3 longitudinal variables for 2 sec reaction delay/1 sec actuation interval without thrust command double.

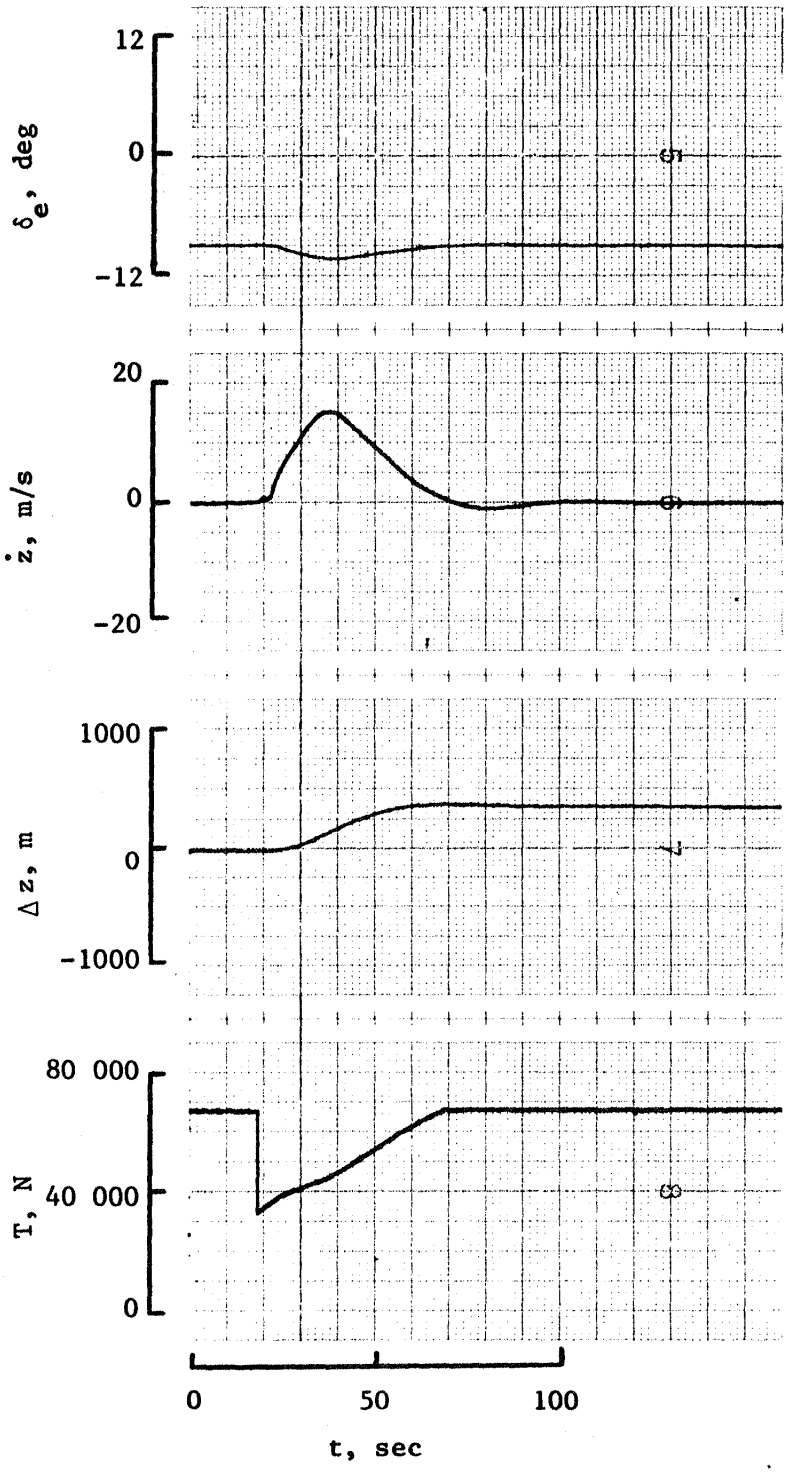

Figure 15. - Concluded.

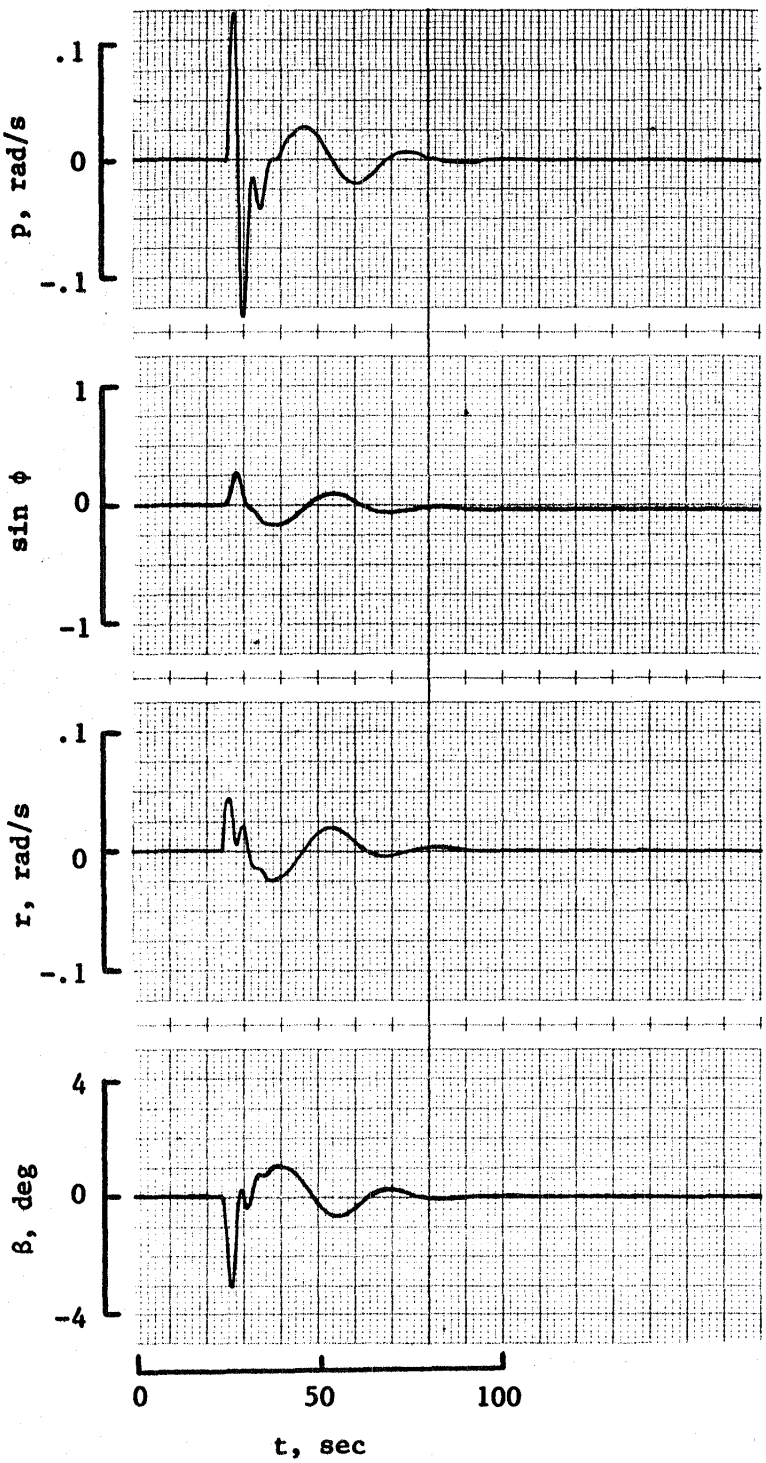

Figure 16. - Condition 3 lateral variables for 2 sec reaction delay/1 sec actuation interval without thrust command double.

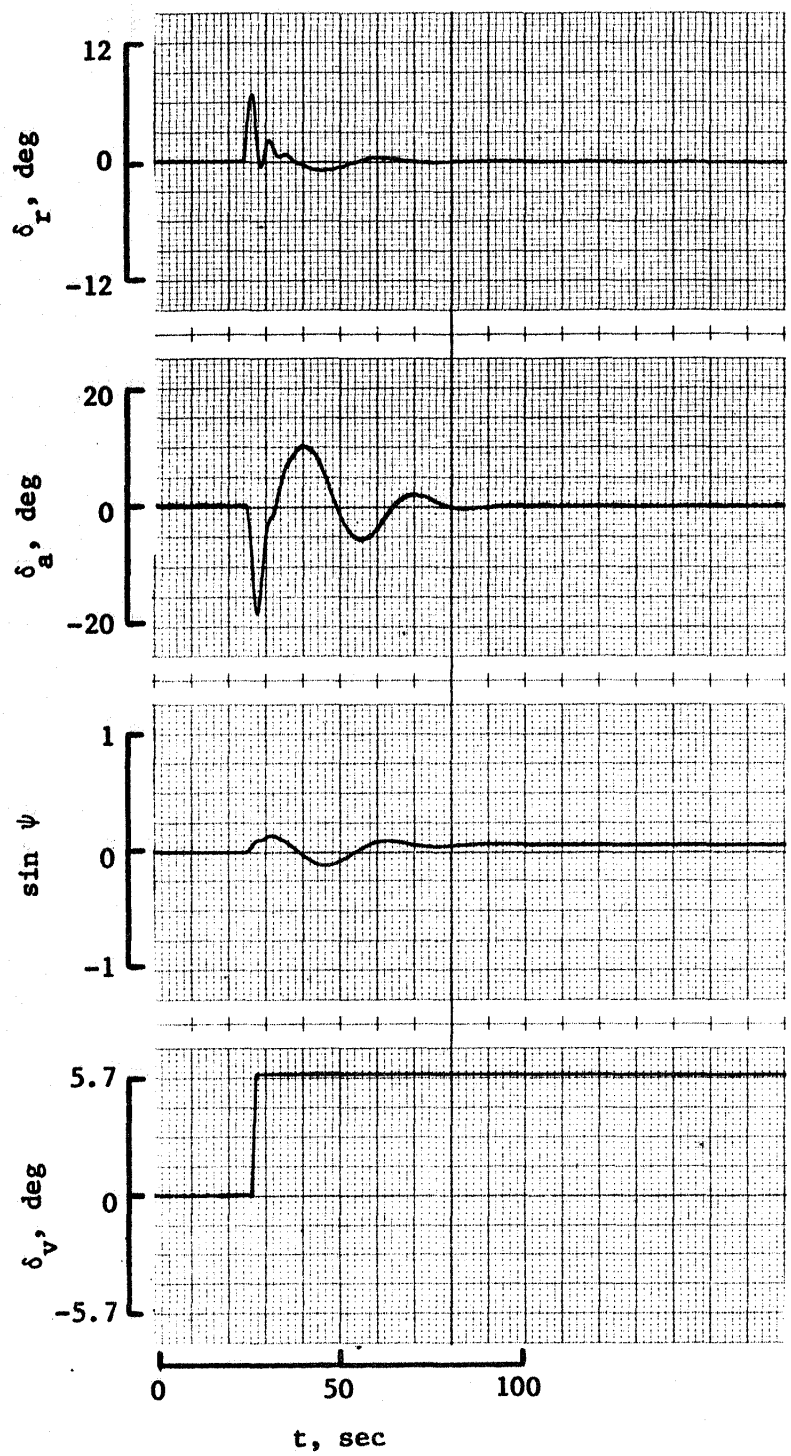

Figure 16. - Concluded.

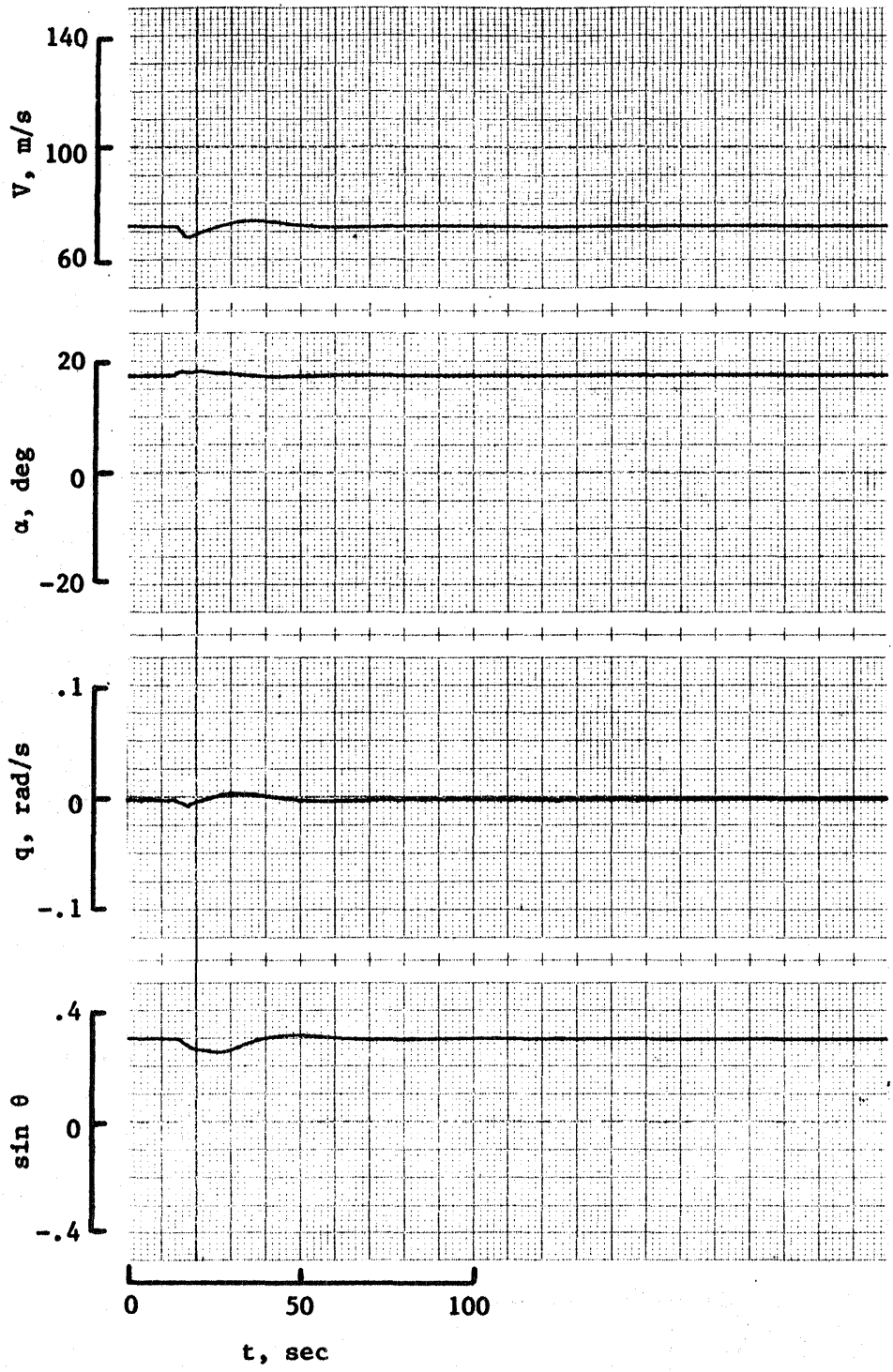

Figure 17. - Condition 3 longitudinal variables for 2 sec reaction delay/1 sec actuation interval with thrust command double.

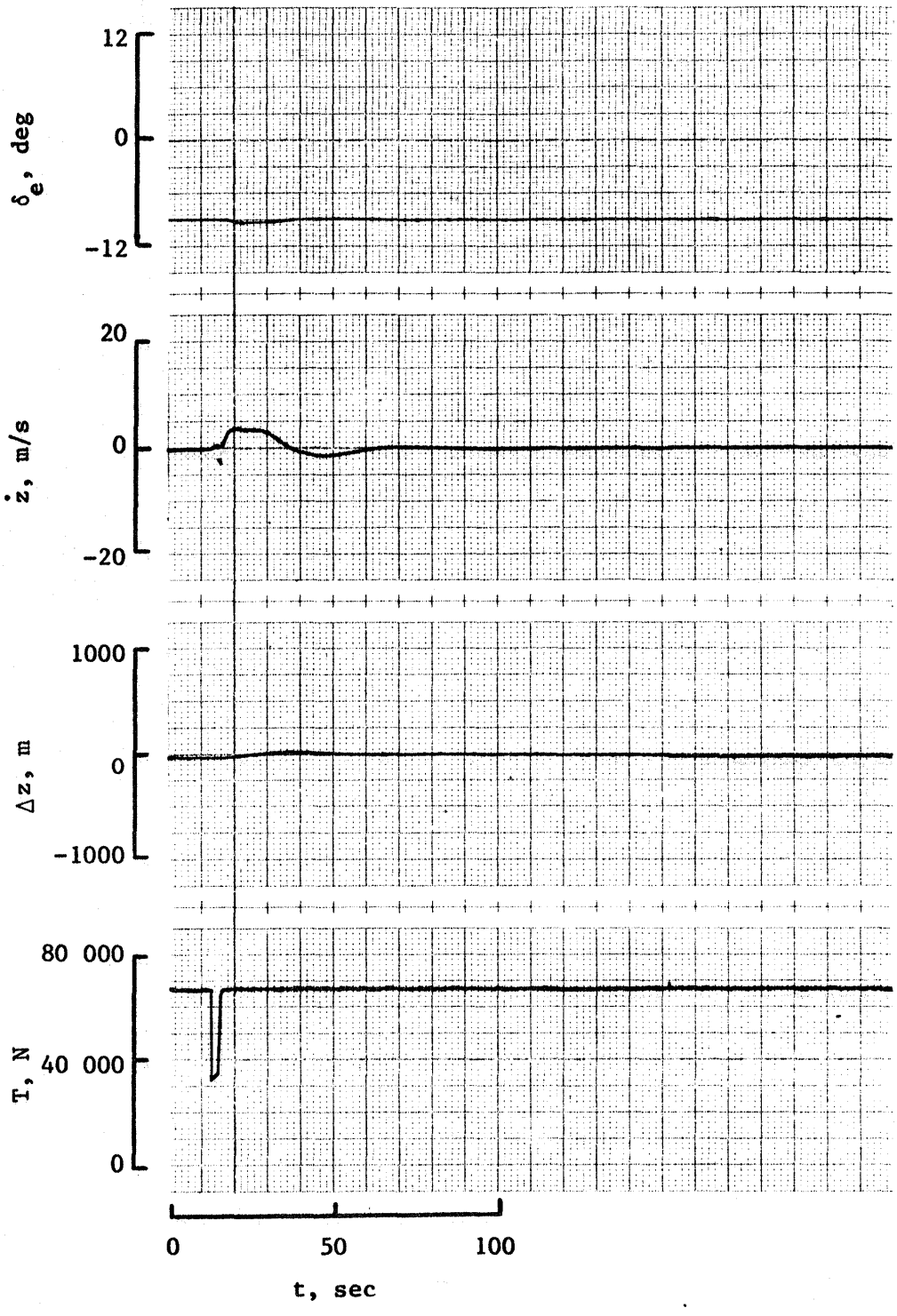

Figure 17. - Concluded.

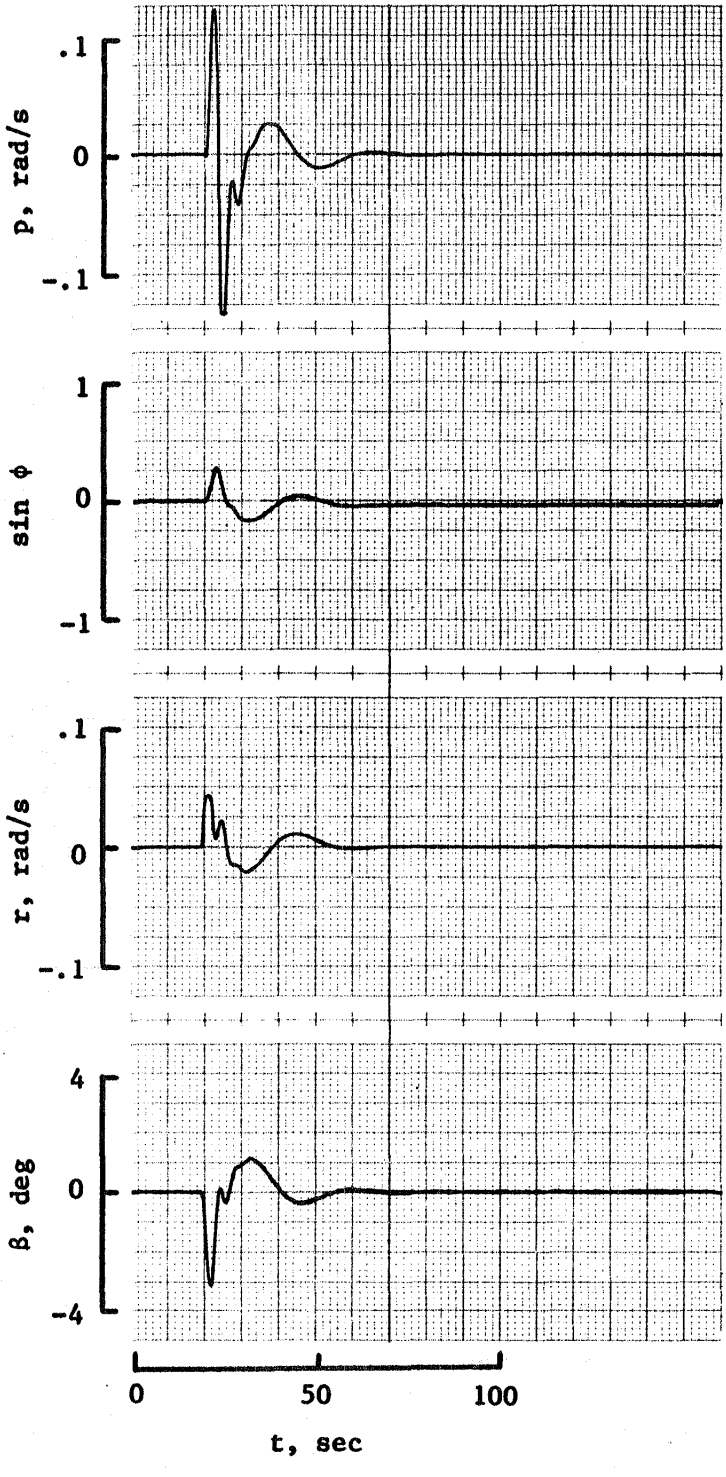

Figure 18. - Condition 3 lateral variables for 2 sec reaction delay/1 sec actuation interval with thrust command double.

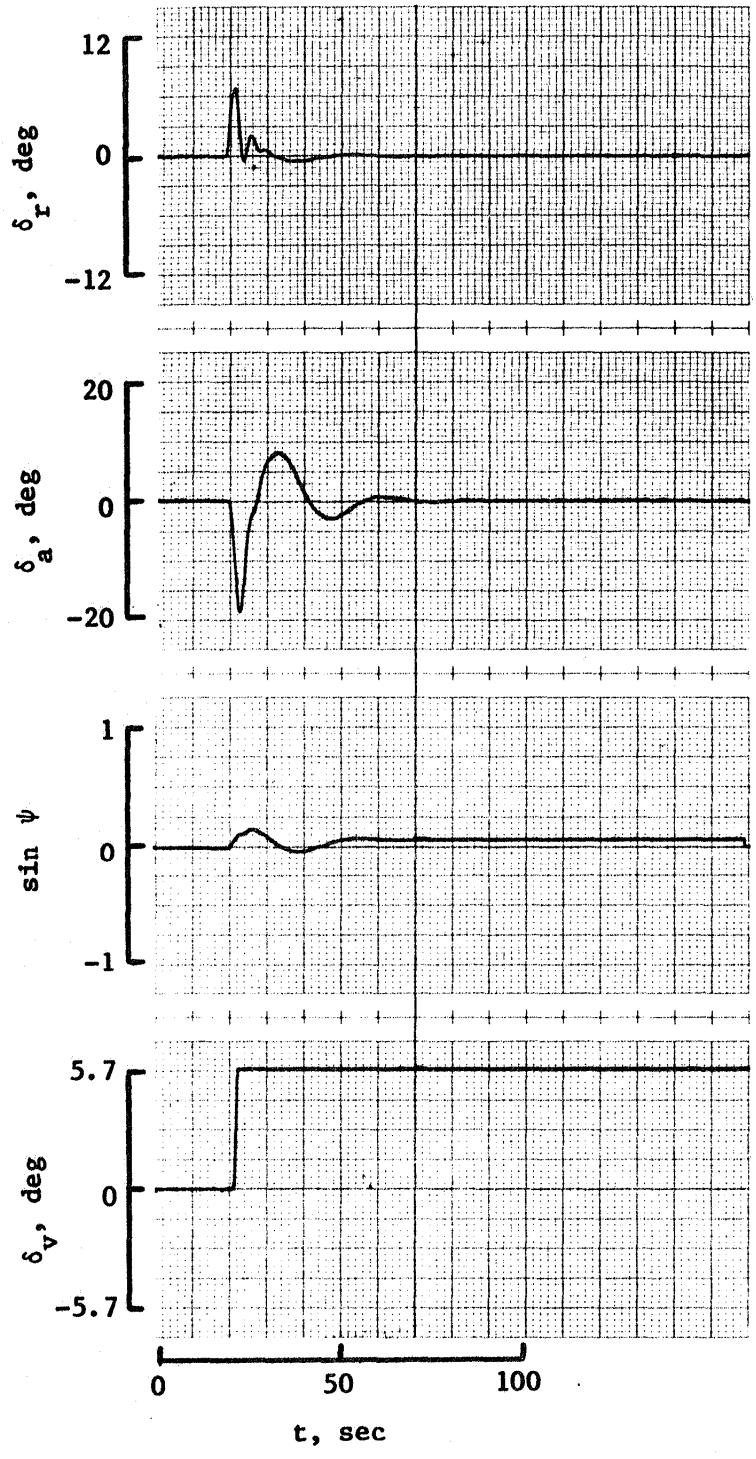

Figure 18. - Concluded.

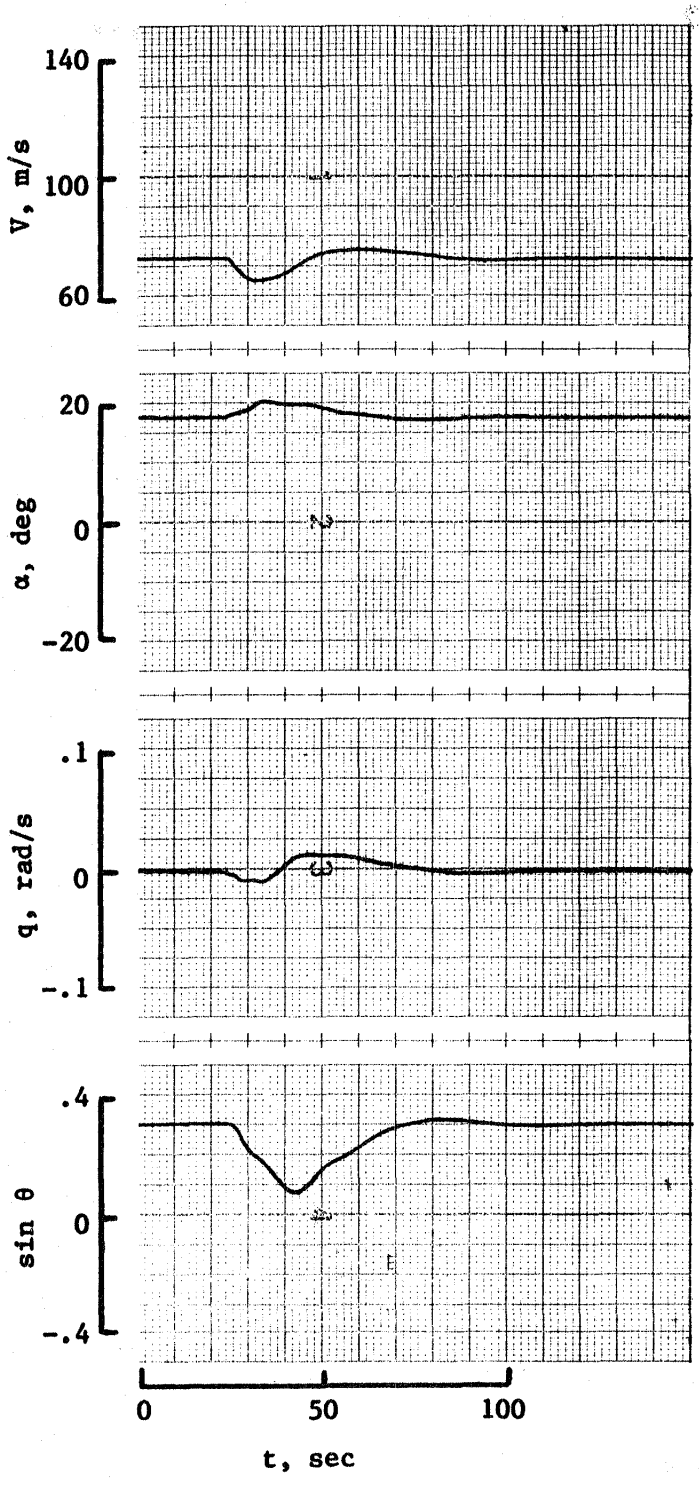

Figure 19. - Condition 3 longitudinal variables for 4 sec reaction delay/2 sec actuation interval without thrust command double.

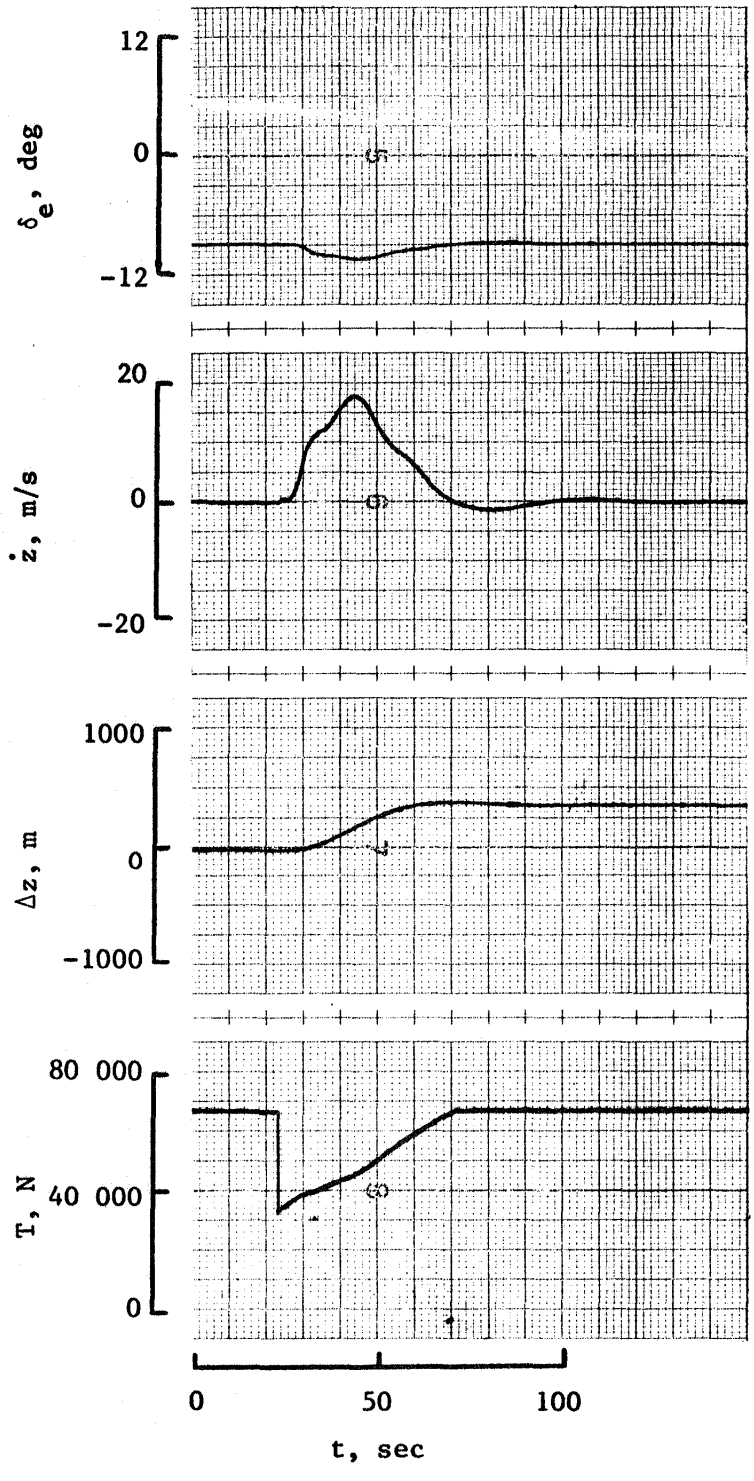

Figure 19. - Concluded.

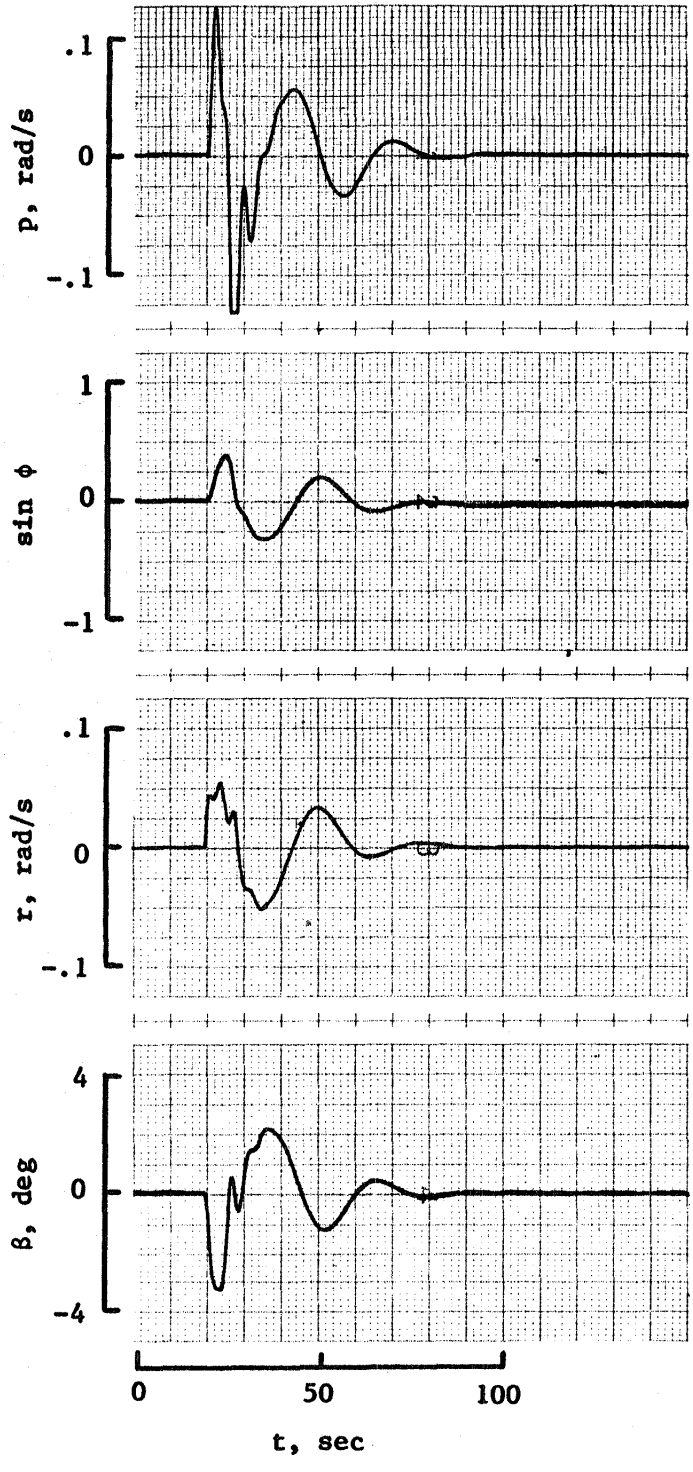

Figure 20. - Condition 3 lateral variables for 4 sec reaction delay/2 sec actuation interval without thrust command double.

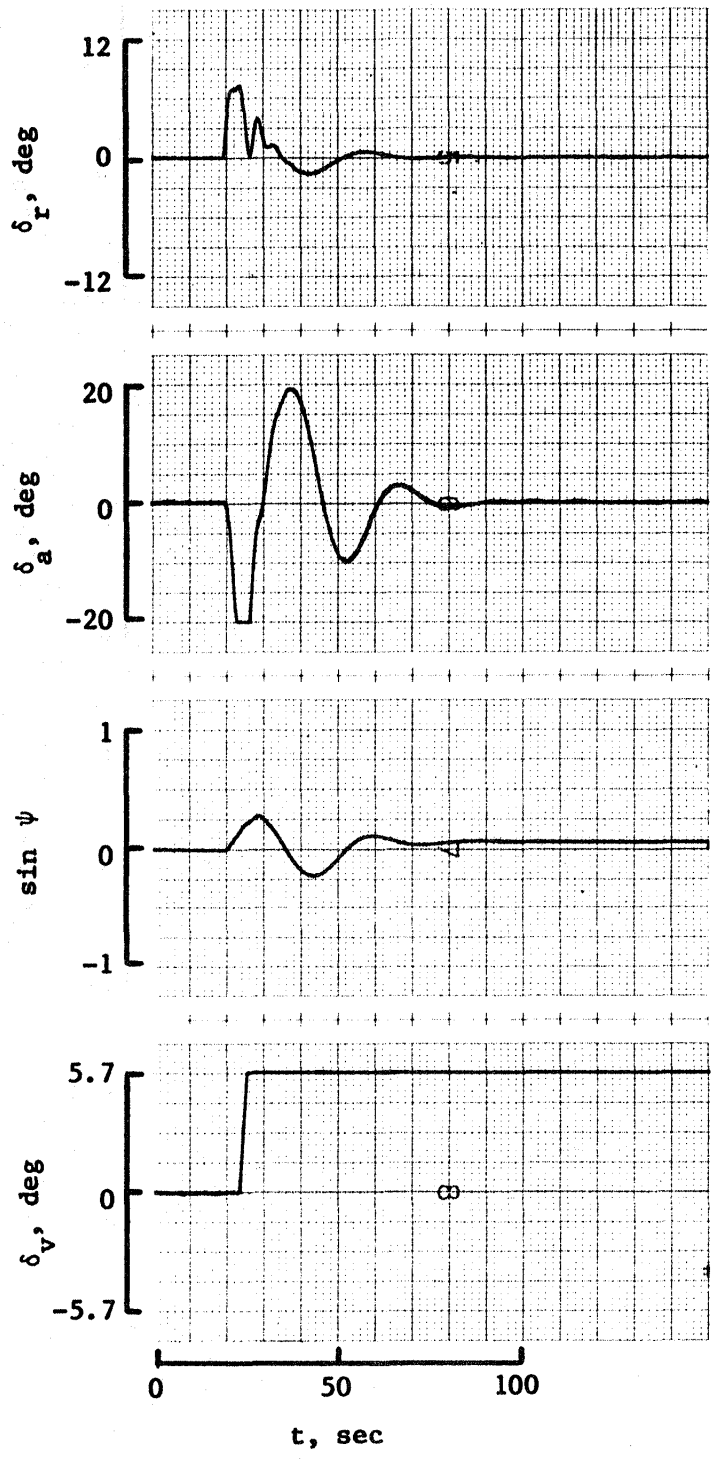

Figure 20. – Concluded.

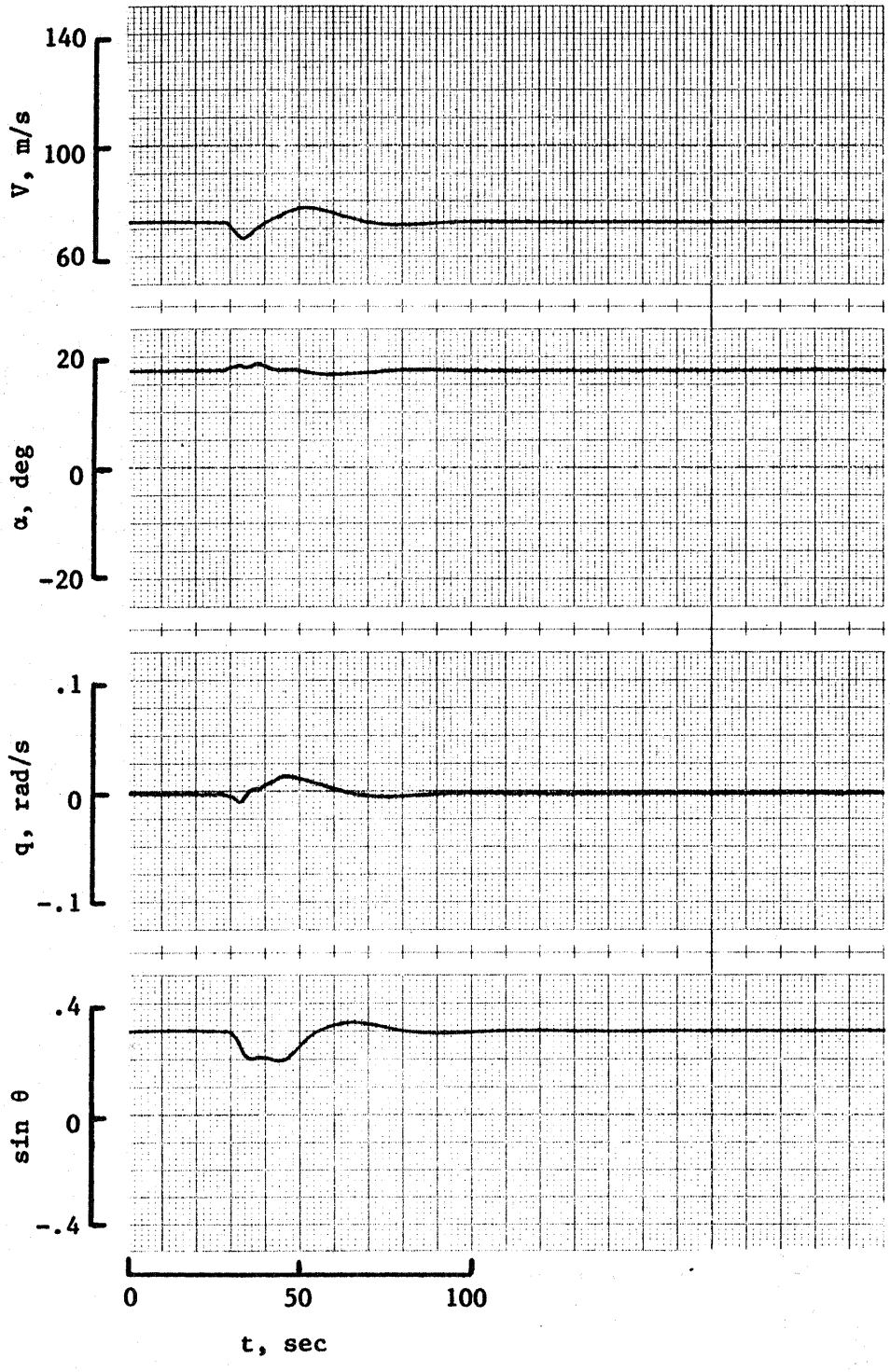

Figure 21. - Condition 3 longitudinal variables for 4 sec reaction delay/2 sec actuation interval with thrust command double.

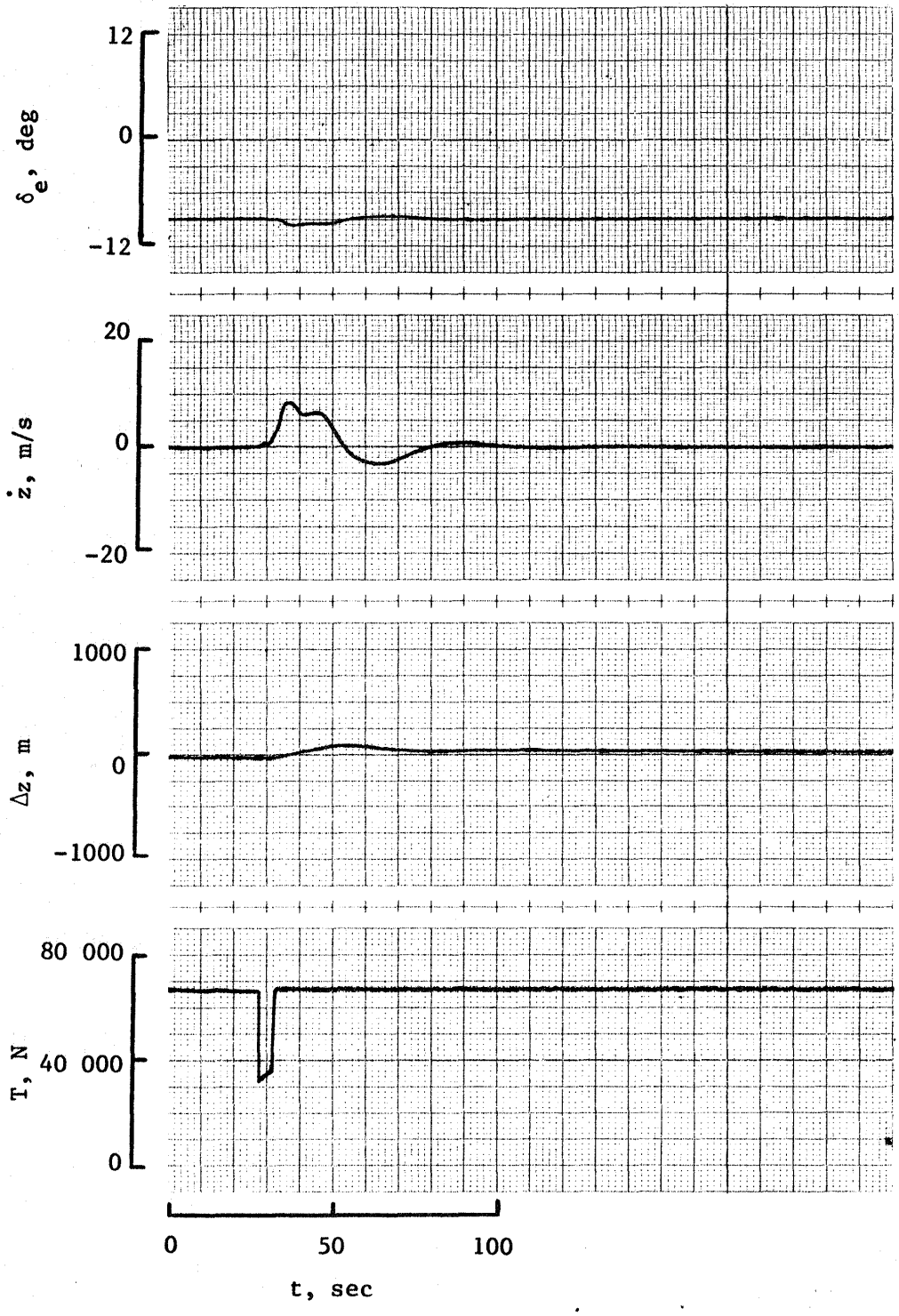

Figure 21. - Concluded.

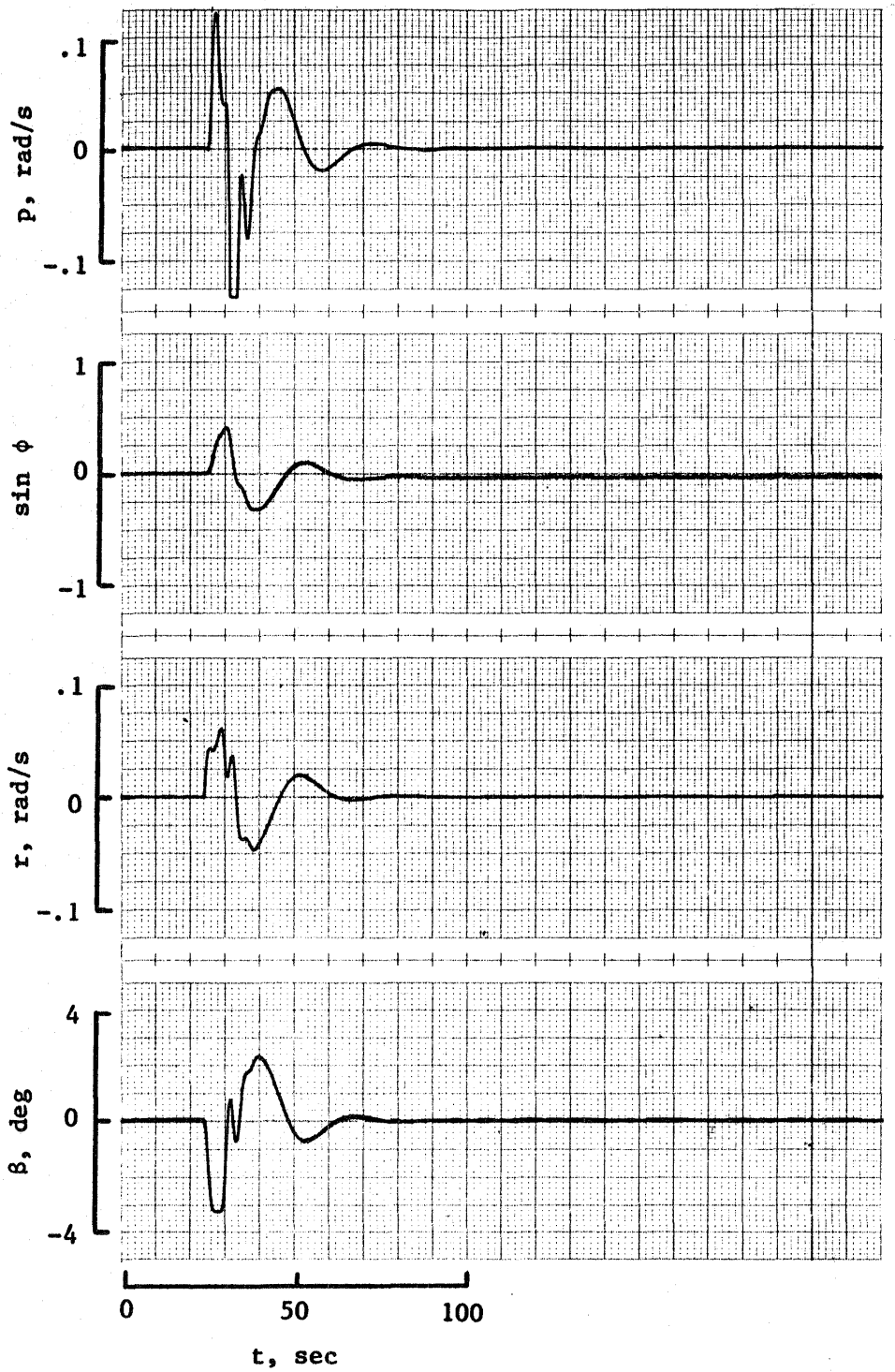

Figure 22. - Condition 3 lateral variables for 4 sec reaction delay/2 sec actuation interval with thrust command double.

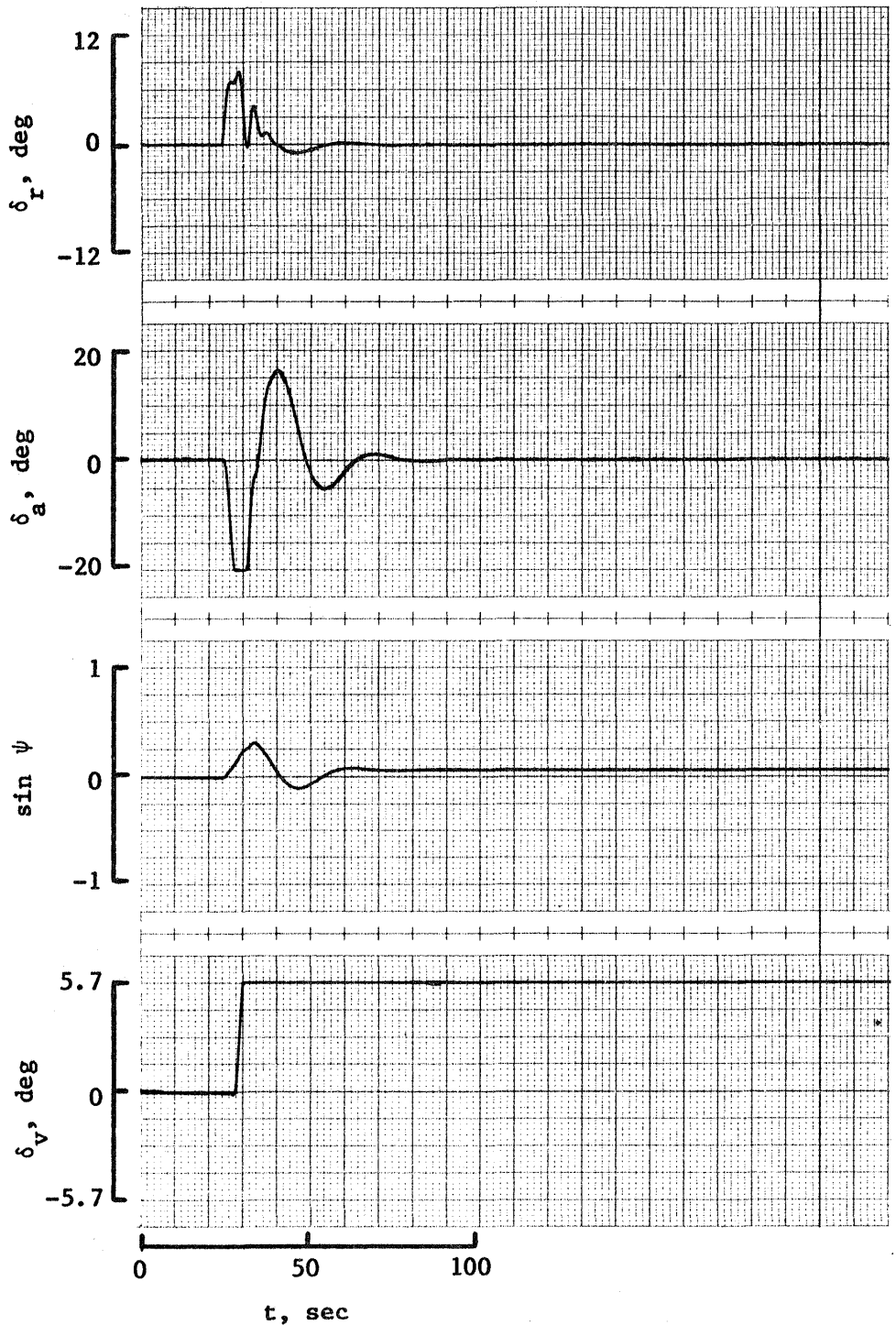

Figure 22. - Concluded.

1. Report No.	2. Government Accession No.	3. Recipient's Catalog No.
NASA CR-166047		

4. Title and Subtitle	5. Report Date
The Use of Laterally Vectored Thrust to Counter Thrust Asymmetry in a Tactical Jet Aircraft	January 1983
	6. Performing Organization Code
7. Author(s)	8. Performing Organization Report No.
J. R. Simons	
	10. Work Unit No.
9. Performing Organization Name and Address	11. Contract or Grant No.
Joint Institute for Advancement of Flight Sciences George Washington University Hampton, VA 23665	NCC1-29
	13. Type of Report and Period Covered
12. Sponsoring Agency Name and Address	Contractor Report Oct. 80 through Oct. 82
National Aeronautics and Space Administration Washington, DC 20546	14. Sponsoring Agency Code

15. Supplementary Notes

Langley Technical Monitor: Frederick J. Lallman
Final Report

16. Abstract

A nonlinear, six degree-of-freedom flight simulator for a twin engine tactical jet was built on a hybrid computer to investigate lateral vectoring of the remaining thrust component for the case of a single engine failure at low dynamic pressures. Aircraft control was provided by an automatic controller rather than a pilot, and thrust vector control was provided by an open-loop controller that deflected a vane (located on the periphery of each exhaust jet and normally streamlined for non-interference with the flow). Lateral thrust vectoring decreased peak values of lateral control deflections, eliminated the requirement for steady-state lateral aerodynamic control deflections, and decreased the amount of altitude lost for a single engine failure.

17. Key Words (Suggested by Author(s))	18. Distribution Statement
Thrust Vector Control Engine Out Twin Engine Tactical Jet Minimum Control Airspeed	Unclassified - Unlimited Subject Category 08

19. Security Classif. (of this report)	20. Security Classif. (of this page)	21. No. of Pages	22. Price
Unclassified	Unclassified	96	A05

For sale by the National Technical Information Service, Springfield, Virginia 22161

End of Document